



**UNIVERSIDAD DE INVESTIGACIÓN DE
TECNOLOGÍA EXPERIMENTAL YACHAY**

Escuela de Ciencias Biológicas e Ingeniería

**TÍTULO: Semiconductor nanoparticles. A review on
recent advances in green chemistry synthesis and their
application in imaging**

Trabajo de integración curricular presentado como requisito
para la obtención del título de Ingeniera Biomédica

Autora:

Mendoza Lescano Lupe Margarita

Tutor:

Ph. D. Ávila Edward

Urcuquí, agosto 2020

Urququí, 2 de septiembre de 2021

SECRETARÍA GENERAL
(Vicerrectorado Académico/Cancillería)
ESCUELA DE CIENCIAS BIOLÓGICAS E INGENIERÍA
CARRERA DE BIOMEDICINA
ACTA DE DEFENSA No. UITEY-BIO-2021-00033-AD

A los 2 días del mes de septiembre de 2021, a las 11:30 horas, de manera virtual mediante videoconferencia, y ante el Tribunal Calificador, integrado por los docentes:

Presidente Tribunal de Defensa	Dr. ALEXIS FRANK , Ph.D.
Miembro No Tutor	Dr. TERCENIO THIBAUT , Ph.D.
Tutor	Dr. AVILA SOSA, EDWARD EBNER , Ph.D.

El(la) señor(ita) estudiante **MENDOZA LESCANO, LUPE MARGARITA**, con cédula de identidad No. **1726070673**, de la **ESCUELA DE CIENCIAS BIOLÓGICAS E INGENIERÍA**, de la Carrera de **BIOMEDICINA**, aprobada por el Consejo de Educación Superior (CES), mediante Resolución **RPC-SO-43-No.496-2014**, realiza a través de videoconferencia, la sustentación de su trabajo de titulación denominado: **Semiconductor nanoparticles. A review on recent advances in green chemistry synthesis and their application in imaging**, previa a la obtención del título de **INGENIERO/A BIOMÉDICO/A**.

El citado trabajo de titulación, fue debidamente aprobado por el(los) docente(s):

Tutor	Dr. AVILA SOSA, EDWARD EBNER , Ph.D.
--------------	--------------------------------------

Y recibió las observaciones de los otros miembros del Tribunal Calificador, las mismas que han sido incorporadas por el(la) estudiante.

Previamente cumplidos los requisitos legales y reglamentarios, el trabajo de titulación fue sustentado por el(la) estudiante y examinado por los miembros del Tribunal Calificador. Escuchada la sustentación del trabajo de titulación a través de videoconferencia, que integró la exposición de el(la) estudiante sobre el contenido de la misma y las preguntas formuladas por los miembros del Tribunal, se califica la sustentación del trabajo de titulación con las siguientes calificaciones:

Tipo	Docente	Calificación
Miembro Tribunal De Defensa	Dr. TERCENIO THIBAUT , Ph.D.	10,0
Tutor	Dr. AVILA SOSA, EDWARD EBNER , Ph.D.	9,9
Presidente Tribunal De Defensa	Dr. ALEXIS FRANK , Ph.D.	10,0

Lo que da un promedio de: **10 (Diez punto Cero)**, sobre 10 (diez), equivalente a: **APROBADO**

Para constancia de lo actuado, firman los miembros del Tribunal Calificador, el(la) estudiante y el(la) secretario ad-hoc.

Certifico que *en cumplimiento del Decreto Ejecutivo 1017 de 16 de marzo de 2020, la defensa de trabajo de titulación (o examen de grado modalidad teórico práctica) se realizó vía virtual, por lo que las firmas de los miembros del Tribunal de Defensa de Grado, constan en forma digital.*



MENDOZA LESCANO, LUPE MARGARITA
Estudiante



FRANK ALEXIS

Dr. ALEXIS FRANK , Ph.D.
Presidente Tribunal de Defensa

Digitally signed by EDWARD EBNER AVILA SOSA
 Date: 2021.09.02 13:43:24 -05'00'

Dr. AVILA SOSA, EDWARD EBNER , Ph.D.
Tutor

THIBAUT
TERENCIO

Firmado digitalmente por THIBAUT TERENCIO
DNI: 70190000
Fecha: 2021.05.02 12:56:52 -05'00'

Dr. TERENCIO THIBAUT, Ph.D.

Miembro No Tutor

KARLA ESTEFANIA ALARCON FELIX

Firmado digitalmente por KARLA ESTEFANIA ALARCON FELIX
Fecha: 2021.05.02 12:56:52 -05'00'

ALARCON FELIX, KARLA ESTEFANIA

Secretario Ad-hoc

SECRETARÍA GENERAL
(Viceministerio Académico/Carrera)

ESCUELA DE CIENCIAS BIOLÓGICAS E INGENIERÍA
CARRERA DE BIOMEDICINA
ACTA DE DEFENSA No. UITEY-BIO-2021-0008

A los 2 días del mes de septiembre de 2021, a las 11:30 horas, de manera virtual mediante videoconferencia, el Tribunal Calificador, integrado por los docentes:

Presidente Tribunal de Defensa: DR. ALEXIS FRANK, Ph.D.
Miembro No Tutor: DR. TERENCIO THIBAUT, Ph.D.
Tutor: DR. AVILA SOSA, EDWARD ERNER, Ph.D.

El/la señor/ta estudiante MENDOZA LESCANO, LUPE MARGARITA, con cédula de identidad No. 1728070673, de la ESCUELA DE CIENCIAS BIOLÓGICAS E INGENIERÍA de la Carrera de BIOMEDICINA, aprobada por el Consejo de Educación Superior (CES), mediante Resolución RRC-80-43-No.488-2014, realiza a través de videoconferencia, la sustentación de su trabajo de titulación denominado: "Semicondutor nanoporosos. A review on recent advances in green chemistry synthesis and their application in imaging", previa a la obtención del título de INGENIERO(A) BIOMEDICINA.

El citado trabajo de titulación, fue decididamente aprobado por el/los docente/s:

Tutor: DR. AVILA SOSA, EDWARD ERNER, Ph.D.

Y recibió las observaciones de los otros miembros del Tribunal Calificador, las mismas que han sido incorporadas por el/la estudiante.

Previamente cumplidos los requisitos legales y reglamentarios, el trabajo de titulación fue sustentado por el/la estudiante y examinado por los miembros del Tribunal Calificador. Escuchada la sustentación del trabajo de titulación a través de videoconferencia, que integró la exposición de el/la estudiante sobre el contenido de la misma y las preguntas formuladas por los miembros del Tribunal, se califica la sustentación del trabajo de titulación con las siguientes calificaciones:

Tipo	Docente	Calificación
Miembro Tribunal De Defensa	DR. TERENCIO THIBAUT, Ph.D.	10.0
Tutor	DR. AVILA SOSA, EDWARD ERNER, Ph.D.	8.9
Presidente Tribunal De Defensa	DR. ALEXIS FRANK, Ph.D.	10.0

Lo que da un promedio de: 10 (Diez punto Cero), sobre 10 (diez), equivalente a: APROBADO

Para constancia de lo actuado, firman los miembros del Tribunal Calificador, el/la estudiante y el/la secretario ad-hoc.

Carístico que en cumplimiento del Decreto Ejecutivo 1017 de 18 de marzo de 2020, la defensa de titulación de examen de grado modalidad técnico práctico se realizó vía virtual, por lo que las firmas de los miembros del Tribunal de Defensa de Grado, constan en forma digital.

MENDOZA LESCANO, LUPE MARGARITA
Estudiante



DR. ALEXIS FRANK, Ph.D.
Presidente Tribunal de Defensa

EDWARD ERNER
AVILA SOSA

DR. AVILA SOSA, EDWARD ERNER, Ph.D.
Tutor

AUTORÍA

Yo, **LUPE MARGARITA MENDOZA LESCANO**, con cédula de identidad 1726070673, declaro que las ideas, juicios, valoraciones, interpretaciones, consultas bibliográficas, definiciones y conceptualizaciones expuestas en el presente trabajo; así como, los procedimientos y herramientas utilizadas en la investigación, son de absoluta responsabilidad de el/la autora (a) del trabajo de integración curricular. Así mismo, me acojo a los reglamentos internos de la Universidad de Investigación de Tecnología Experimental Yachay.

Urququí, septiembre 2021.



Lupe Margarita Mendoza Lescano

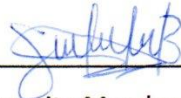
CI: 1726070673

AUTORIZACIÓN DE PUBLICACIÓN

Yo, **LUPE MARGARITA MENDOZA LESCANO**, con cédula de identidad 1726070673, cedo a la Universidad de Investigación de Tecnología Experimental Yachay, los derechos de publicación de la presente obra, sin que deba haber un reconocimiento económico por este concepto. Declaro además que el texto del presente trabajo de titulación no podrá ser cedido a ninguna empresa editorial para su publicación u otros fines, sin contar previamente con la autorización escrita de la Universidad.

Asimismo, autorizo a la Universidad que realice la digitalización y publicación de este trabajo de integración curricular en el repositorio virtual, de conformidad a lo dispuesto en el Art. 144 de la Ley Orgánica de Educación Superior

Urququí, septiembre 2021.



Lupe Margarita Mendoza Lescano

CI: 1726070673

Acknowledgements

En primer lugar, agradezco a Dios por darme sabiduría y guiarme durante este largo camino. Porque Su diestra me sostuvo, fue mi amparo y fortaleza, mi pronto auxilio en las tribulaciones. Fue Él quien puso en mi camino a personas extraordinarias en mi vida:

Lupe Dávalos, mi abuela que, con mucho amor y disciplina, ha cuidado de mí y de mi educación. Acompañándome con constante desvelo desde mis 8 años. Inmensas gratitud y deuda por cuidar de Mateo, Shyrley, Gina, Juan y Lucas. De no haber sido por ella, no sé qué hubiera sido de mí y de mis hermanos. *Juan Carlos Ponce*, la figura paterna que siempre necesité, quién me acompañó en mis logros y derrotas. *Gloria Navas*, su gran amistad desinteresada reflejada en sus oraciones, llamadas y preocupación por mí. *Eduardo Ortega*, sus consejos paternos y ayuda en mi crecimiento personal. *Carlos Cocha*, compañero y mejor amigo que me motivó cada día a dar lo mejor de mí, el enseñarme su forma de interpretar el universo usando la física, la ecuación de Dirac, por ejemplo. No olvidaré el increíble equipo que fuimos. A *mi familia*, los *Andrade González*, su apoyo y confianza permitieron que concluya esta tesis satisfactoriamente. Vivir con ustedes simplemente me hace feliz. Gracias por ayudarme a cumplir mis objetivos como persona y estudiante. A *Paola Andrade*, mi mejor amiga. Nunca encontraré a nadie más leal. Mi eterna gratitud por alentarme y brindarme tu amistad desde los once años. Sigamos viéndonos crecer la una a la otra.

Agradezco enormemente a *Edward Ávila*, mi tutor quién, con su amplio conocimiento me encaminó durante mi titulación. Gracias por su completa disposición y soporte desde el comienzo. Cada aporte a mi tesis y defensa fue incalculable. Dios le bendiga.

Un especial agradecimiento a *Si Amar Dahoumane*, uno de los primeros profesores que tuve. Su afán por enseñar, su ambición por la calidad científica, su disposición para sus estudiantes. Gracias por ser un increíble científico, amigo y tutor.

Gracias *my Emily G.* Por ser mi amiga y ayudarme tantas veces cuando caí, por no juzgarme, por ser incondicional. Queridos *Vicky S., Katty V., Oscar Y., Gene G., Cris P., Lady R.* y *Nicky L.*, por hacer de mi vida universitaria más llevadera desde que comenzó y a *David C.* por cerrar con broche de oro tan caótica y feliz época. Gracias por salvarme la vida y permanecer conmigo incluso después de sentir la muerte. Todos ustedes son mis únicos y mejores amigos. Los amo por siempre.

Mi eterno agradecimiento

Lupe Margarita Mendoza Lescano

Dedico este trabajo

A las personas que amo. Por su soporte, motivación y cariño. Por demoler y construir todo lo que soy ahora. Por resistir conmigo el caos del pasado, y el venidero.

A Mateo, Shyrley, Juan, Gina y Lucas. ¡Qué mayor motivación para ustedes, que su hermana mayor lo lograra! Cada uno de mis logros es suyo.

Al pequeño-gran desastre, jamás pusilánime, que vive en contrariedad con el mundo, yo.

Lupe Margarita Mendoza Lescano

Resumen

Hasta la fecha, la preparación y las aplicaciones de nanopartículas basadas en semiconductores se han estudiado y desarrollado ampliamente. Sin embargo, esta revisión se centra en los desarrollos, avances más recientes de puntos cuánticos semiconductores que se pueden emitir principalmente en las regiones del infrarrojo cercano (NIR-I y NIR-II); relacionándolo con la imagenología como una aplicación biomédica versátil para el diagnóstico de un sinnúmero de enfermedades. Estos desarrollos permiten identificar cuál de todos los métodos más recientes permiten la síntesis de dichos materiales y su aplicación. Primero, esta revisión compila la información de la literatura relacionada con semiconductores, teoría de bandas, región del infrarrojo cercano, imagenología siendo la aplicación biomédica seleccionada de este trabajo, sus técnicas y sus derivados, Segundo, este escrito describe las preparaciones más actuales de nanopartículas basadas en semiconductores y, en tercer lugar, la posible mejora usando la síntesis química verde como una alternativa amigable con el ambiente. Además, se discuten los desafíos y los problemas actuales respecto a la morfología, reactivos y síntesis de las nanopartículas, Finalmente, este ensayo concluye discutiendo las futuras perspectivas y líneas de investigación para las estructuras nanométricas revisadas.

Palabras Clave: Semiconductores, nanopartículas, puntos cuánticos, química verde, nanotecnología, imagenología.

Abstract

To date, the preparation and applications of semiconductor nanoparticles have been widely studied and developed. However, this review focuses on the most recent advancements of semiconductor QDs that can mainly emit in the NIR-I and NIR-II regions, relating it to imaging as a versatile biomedical application and analyzing which of all the most recent methods allows to synthesize said material and thus to use it. First, this review compiles the information from the literature related to semiconductors, quantum dots, band theory, near-infrared region, imaging being the selected biomedical application of this work, and addresses its techniques, their shortcomings, threats, and opportunities. Second, this paper describes the most current preparations of nanoparticles based on semiconductors and, thirdly, the possible improvement using green chemical synthesis as an environmentally friendly alternative. The current challenges and problems regarding the morphology, reagents, and synthesis of nanoparticles are also discussed. Finally, this essay concludes by discussing the future perspectives and investigation lines for the revised nanometric structures.

Key words: Semiconductors, nanoparticles, quantum dots, green chemistry, nanotechnology, imaging.

Contents

List of Figures.....	XI
List of Tables.....	XII
List of Abbreviations.....	XIII
Chapter I 1	
1. Introduction	1
1.1 Semiconductors in the nanoworld.....	1
1.2 Imaging.....	9
2.1 Problem Statement	15
1.4 General and Specific Objectives	16
Chapter II 17	
2. Semiconductor nanoparticles.....	17
2.1 IV Group	19
2.2 III-V Group	22
2.3 II-VI Group	27
2.4 I-VI Group.....	30
2.5 I-III-VI Group	31
2.6 IV-VI Group.....	32
2.8 Layered Semiconductors	33
Chapter III 39	
3 Chemical method vs Green method.....	39
3.1 Green Synthesis (either from plant extracts or from nutrients).....	39
Chapter IV 44	
Conclusion and Outlook	44
Annexes 45	
References 47	

List of Figures

Figure 1. Semiconductors of the periodic table. This section contains semiconductor elements. The most common semiconductor materials are highlighted in green.....	2
Figure 2. The molecular orbitals in a bulk material are depicted in detail.	6
Figure 3. Intrinsic semiconductor diagram.....	7
Figure 4. N-type semiconductor and its band structure.	8
Figure 5. P-type semiconductor diagram and its band structure.	9
Figure 6. Behavior of (A) Direct and (B) Indirect Band Gap Semiconductors.....	10
Created with BioRender.com	10
Figure 7. Schematic of typical QDs structure containing a fluorescent core, wide bandgap semiconductor shell, surface ligands, and their and QDs imaging systems. ...	18
Figure 8. Semiconductors from group IV of the periodic table.....	19
Figure 9. Semiconductors from either elements or combinations of group III and group V (called III-V semiconductors).	24
Figure 10. Semiconductors from either elements or combinations of group II B and group VI A (called II-VI semiconductors).	29
Figure 11. Semiconductors from either elements or combinations of group IV and group VI (called IV-VI semiconductors).....	33
Figure 12. Synthesis classification for nanoparticles as a whole.....	42
Figure 13. Green synthesis vs. Different synthetic methods. Main characteristics.....	43

List of Tables

Table 1. Traditional elemental semiconductor according to the periodic table and some compound semiconductors including layered semiconductors.....	3
Table 2. Most common modalities for various types of imaging tests.....	11
Table 3. Updated methods of Si QDs synthesis for bioimaging. A comparison of synthetic conditions for preparing Si nanostructures with different precursors, solvents, reactions, and conditions for the green chemical method.	23
Table 4. Updated methods of BN synthesis for bioimaging. A comparison of synthetic conditions for preparing h-BN nanostructures with different precursors, solvents, reactions, and conditions for the green chemical method.	28
Table 5. Updated methods of BP synthesis for bioimaging. A comparison of synthetic conditions for preparing BP nanostructures with different precursors, solvents, reactions, and methods.	37
Table 6. Overall classification of semiconductors according to their group, alloys and structure.	45

List of Abbreviations

- 2D:** two-dimensional
- BNNTs:** Boron Nitride Nanotubes
- BNNFs:** Boron Nitride Nanoflakes
- BOCVD:** Boron Oxide Chemical Vapour Deposition
- BP:** Black Phosphorus
- CT:** Computed Tomography
- CVD:** Chemical Vapor Deposition
- DFM:** Dimethylformamide
- DMSO:** Dimethyl Sulfoxide
- EEG:** Electroencephalography
- EKG:** Electrocardiography
- EPR:** Enhanced Permeability and Retention
- FL:** Fluorescence
- FLBP:** Few-Layer Black Phosphorus
- GO:** Graphene Oxide
- h-BN:** Hexagonal Boron Nitride
- HEMM:** High Energy Mechanical Milling
- ICG:** Indocyanine Green
- LDH:** Layered Double Hydroxides
- LPE:** Liquid-Phase Exfoliation
- MEG:** Magnetoencephalography
- MRI:** Magnetic Resonance Imaging
- NIR:** Near-Infrared Region
- NMP:** N-methyl Pyrrolidone
- NPs:** Nanoparticles
- NR:** Nanorod
- NTs:** Nanotubes

ODCB: *o*-dichlorobenzene

PA: Photoacoustic

PBS: Phosphate-Buffered Saline

PDT: Photodynamic Therapy

PEG: Polyethylene Glycol

PET: Positron Emission Tomography

PLGA: Poly Lactic-co-Glycolic Acid

Ppm: parts-per-million

PTT: Photothermal Treatment

PVP: Poly (vinylpyrrolidone)

QDs: Quantum Dots

SC: Semiconductors

SERS: Surface-Enhanced Raman Scattering

SWIR: Short-wavelength Infrared Region

TiL4: Titanium sulfonate Ligand

TMDCs: Transition Metal Dichalcogenides

VDW: Van Der Waals

Chapter I

1. Introduction

1.1 Semiconductors in the nanoworld.

When we say *nano*, we must consider this prefix "*nano*," which means "one billionth part" (10^{-9}). This nanometric range includes all types of matter with at least one dimension at a size between 1 and 100 nanometers. Within this range, we have nanotechnology manipulating matter to bring us breakthroughs.

Nanotechnology is known as the manipulation and application of matter on a nanometric scale. Due to this size range, the field of nanotechnology is vast and multidisciplinary, including branches such as semiconductor physics, molecular biology, organic chemistry, inorganic chemistry, engineering, materials, among others. Nanotechnological manipulation makes it possible to obtain research and various associated applications, starting from devices, self-assembled structures, and the development of new nanomaterials. Thanks to the variety of applications mentioned, nanotechnology is a potential branch of study and development at present and, so does at the future. Among the nanomaterials we can find out are the nanocomposites, nanoparticles (NPs), nanotubes (NTs), nanorods (NRs), quantum dots (QDs), nanoporous materials, nanocups, and biological nanostructures^{1,2}.

Another term that deserves to be mentioned is nanomedicine, which is the application of nanotechnology in medicine. Eric Drexler's vision of nanomechanical machines and their future medicine applications gave rise to the term nanomedicine³. This latter covers all aspects of medical nanotechnology; nonetheless, the majority are focused on the regulation and manipulation of processes at the nanoscale, as applied to diagnosis, treatment, and, of course, the potential use of molecular nanotechnology.

Within those nano resources mentioned above, elemental and compound semiconductors (SC) could be manipulated to be integrated at such scale. Those are organic or inorganic materials with an energy gap of less than 4 eV and an electrical conductivity between that

of a metal, such as gold, and an insulator such as glass. So, in few words, these materials have lower electrical conductivities than a metal conductor but higher than a good insulator, although what characterizes them especially are the gaps. Unlike in conductors, semiconductors' electrons must obtain energy (i.e., ionizing radiation) to traverse the bandgap and reach the conduction band.

Since semiconductors are made up of elements from various classes, there are several different types of semiconductors with distinct properties. Besides, different elements within the same group (IV) can form compound semiconductors like Silicon Carbide (SiC). However, the latter, carbon-based SC materials, most of the SC compounds such as triple, quadruple, and quintuple alloys; organic semiconductors, SC polymers; various oxides and magnetic semiconductors will not be discussed in this work. Similarly, concerning layered semiconductors, only black phosphorus (BP) and molybdenum disulfide (MoS₂) will be treated. All these compounds mentioned above are part of a large field of study and must be described in detail in another review.

Elemental semiconductors, B, P, and C, which are derived from elements in groups II, III, and IV of the periodic table, respectively (Fig 1); and compound semiconductors, the most common of which are derived from groups III and V such as GaAs and groups II and VI CdS of the periodic table are displayed in Table 1. This table also displays their corresponding group in the periodic table, their remaining electron laying in their last layer and their band-gap energy, respectively. Moreover, semiconductors can be doped with impurities and activated with electric fields; thus, their conductivity can be increased and regulated. So, the doping allows semiconductors to be classified according to impurities' content as intrinsic and extrinsic.

		IIA	IVA	VA	VIA	VIIA
		⁵ B	⁶ C	⁷ N	⁸ O	⁹ F
IB	IIB	¹³ Al	¹⁴ Si	¹⁵ P	¹⁶ S	¹⁷ Cl
²⁹ Cu	³⁰ Zn	³¹ Ga	³² Ge	³³ As	³⁴ Se	³⁵ Br
⁴⁷ Ag	⁴⁸ Cd	⁴⁹ In	⁵⁰ Sn	⁵¹ Sb	⁵² Te	⁵³ I
⁷⁹ Au	⁸⁰ Hg	⁸¹ Tl	⁸² Pb	⁸³ Bi	⁸⁴ Po	⁸⁵ At

Figure 1. Semiconductors of the periodic table. This section contains semiconductor elements. The most common semiconductor materials are highlighted in green.

Table 1. Traditional elemental semiconductors, according to the periodic table and some compound semiconductors, including layered semiconductors. Those with an * are indirect band gap semiconductors.

Features	Elemental Semiconductors						
	Cd	Al, B, Ga, In			C, Si, Ge	As, P, Sb	S, Se, Te
Group e ⁻ (last layer)	IIB 2 e ⁻	IIIB 3 e ⁻			IVA 4 e ⁻	VA 5 e ⁻	VIA 6 e ⁻
Band-gap energy (eV)	Compound Semiconductors				Quantum Dots (QDs)		
	II-VI Group	IV-IV Group	IV-VI Group	Ternary Group	III-V Group	IV Group	Layered SC
0.00-1.00	Hg-Te Hg-Se	SiGe	PbSe, PbS	HgCdTe InGaAs	InSb InAs GaSb	Sn Ge*	BN
1.00-2.00	CdTe CdSe	SiGe	SnS	AlInA AlGaAs CdZnTe CdMnTe TiBrI HgBrI	GaAs, InP AlSb BP, InN AlAs GaP*,AlP	Si*	BP
2.00-3.00	HgS ZnTe, CdS ZnSe MnSe MnTe	SiC*					
3.00-4.00	MgTe, MnS MgSe, ZnS ZnO ZnS	α -SiC					
4.00-5.00	MgS						
> 5.00					BN, AlN	C*	

Among SCs most abundant in nature is Silicon (Si) element, which is of the group IV. It represents the second element most abundant on Earth after oxygen. It is also the most frequently used semiconductor. Additionally, Aluminum (Al), cadmium (Cd), phosphorous (P), sulfur (S), germanium (Ge), and selenium (Se) are some other semiconductors. The properties of each semiconductor are determined by the energy gap between the valence and conduction bands⁴.

Concerning to Ecuador semiconductor elements sources, the country is among Antimony mines, deposits, and some minor occurrences similar to countries such as Algeria, Bosnia, Herzegovina, Brazil, and others⁵. In Portobello, Zaruma there is a Silver (Ag) and Ga epithermal deposit. There, the Gallium concentration (ppm) is 0.1⁶. Aluminum could be

obtained by electronics recycling, but its natural occurrence is in Lake Cuicocha water where total aluminum concentration raises to $7.2 \mu\text{mol L}^{-1}$, with nearly 70% occurring as filterable Al at neutral to weakly alkaline conditions⁷. Indium and its derivatives also could be recovered from electronics waste. Another 39.45% of aluminum is found in the aluminum anodizing sludge of an industry that operates in Ecuador. Here comes the idea of feasibility study for the creation of an industrial company dedicated to the manufacture and installation of aluminum from said aluminum waste. Indium and its derivatives⁸ also could be recovered from electronics waste^{9,10}.

Significant concentrations of carbon exist in the form of chemicals. Carbon (C) is found in the atmosphere in the form of carbon dioxide at a concentration of 0.03% by volume. Carbonates are found in a variety of rocks, including granite, dolomite, gypsum, and marble. Complex organic compounds of carbon, hydrogen, oxygen, nitrogen, and other elements make up all living plants and animals. Fuel oil (petroleum), alfalt, and bitumen are soils formed by the remains of living plants and animals. C and H complexes are found in natural gas sources. Petroleum is Ecuador's main export product and one of the main sources of financing for the fiscal budget. Moreover, when pastures are turned to secondary forest or plantation forest in northwestern Ecuador, soil C content increases. Plots of matched pasture and forest were compared at 40 locations throughout the country. Pasture age was the most important element in understanding improvements in C reserves after pasture to woodland conversion¹¹. Forests of pastures older than 30 years had an estimated higher C content of 15.8 Mg ha⁻¹ than pastures. Additionally, reforestation of old pastures would usually result in a rise in soil C stocks in this area.

Geogenic arsenic (As) can build up in rice grains to exceed dangerously high concentrations, posing a risk to human health¹². Ecuador is one of South America's largest rice producers and costumers. However, no data on As concentrations in rice agrosystems is available, despite the fact that certain water bodies are known to contain high amounts of the substance¹³. In all sections of the rice plants, the organic As type is the most prevalent (> 80%)¹⁴. One way to extract As and other compounds concentrated in those stocks could be the use of plants with potential for their phytoextraction. On the other hand, arsenic in geothermal waters in Andean areas ranges from 2–969 g As/L, and sediments contain arsenic in the range of 1.6 to 717.6 mg/kg, according to the findings^{15,16}.

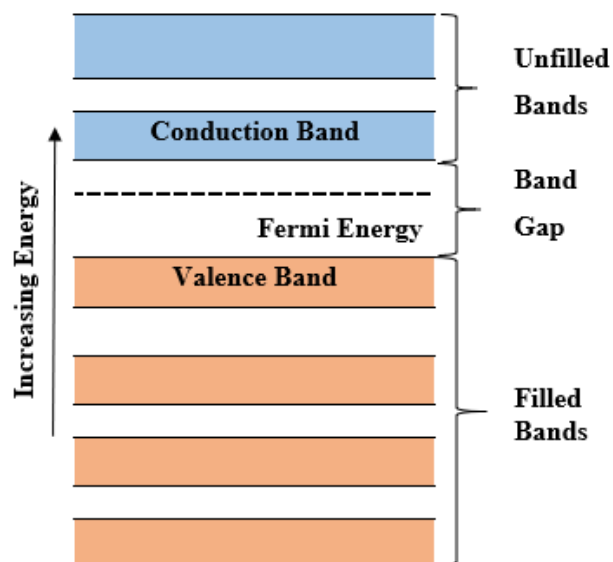
A research forest is situated on the steep slopes of Ecuador's northern Andes showed some organic sources of N, P, and S which contributed 55, 66, and 63%, respectively, to overall N, P, and S concentrations in all ecosystem fluxes. Except for inorganic P and S, the organic layer was the largest source of all N, P, and S bacteria. Phosphorus fractions could be found in mountain soils of southern Ecuador, but only in terms of P^{17,18}.

Fruta del Norte is a totally hidden and protected epithermal gold-silver mine in southeastern Ecuador's Cordillera del C ndor mountain. It ranges. 15.0 million ounces (Moz) of silver are included in currently identified deposits in a single, steep, comparatively narrow body of excellent quality consistency, with an indicated resource grade of 12.9 g/t Ag¹⁹.

Mollusks, crustaceans, cephalopods, and crabs all have high Cd concentrations. Furthermore, oilseeds, wild mushrooms, and cacao contain elevated amounts. Cadmium levels in Ecuadorian soils range from 0.44 (0.03 - 10.0) mg Cd kg⁻¹ soil²⁰. It is common knowledge that Ecuador is full of this diversity of flora and fauna. Therefore, it could be said that they are Ecuadorian sources that have Cd.

One interesting fact is even though the final products are not semiconductor elements, Ecuadorian black mineral sands were used as starting material for the production of iron titanium oxide nanostructures.

In solids, the atoms get so close that their electric orbitals start to overlap spatially, and each atomic level breaks into many neighboring levels, which are energetically close, effectively forming a continuous energy band²¹. An atom has an infinite number of energy



levels, and a solid has an immense number of permitted bands. Nonetheless, the most influential bands and band gaps (relevant for electronics and optoelectronics) are those near The Fermi level, as well as the valence and conduction bands. The valence band can be interpreted as the outermost electron orbital level of an atom occupied by electrons whose significant fraction of electrons can be excited to cross the band gap to reach the conduction band. In the conduction band, the electrons have enough energy to move freely in the material, creating an electric current. In Fig 2. electrons exit the valence band and join the conduction band as the energy rises. The relative band gap distinguishes semiconductors further. The bandgap in semiconductors is small, allowing electrons to nearly fill the conduction band.

Figure 2. The molecular orbitals in a bulk material are depicted in detail.

Semiconductors have a small bandgap (around 3-4 eV). This property allows them to have an intermediate conductivity between conductors and insulators, which is one of the reasons they are good for electric circuits: they would not short out as a normal conductor would. Narrow bandgap materials (InSb, Bi₂Te₃) are used as infrared photodetectors or thermoelectrics (which convert heat to electricity), whereas broader gap materials (Si, GaAs, GaP, GaN, CdTe) are used in electronics, light-emitting diodes, and solar cells. In all these processes, it is the energy absorbed or emitted by electrons passing from the conduction to the valence bands which is used^{22,23}.

1.1.1 Intrinsic Semiconductors

Intrinsic semiconductors or i-type semiconductors are an utterly pure type of semiconductors without any doping species present. They act as insulators at room temperature because it only has a few free electrons and few gaps due to thermal energy. While there are flows of electrons and holes in an intrinsic semiconductor, the total current is zero. Since thermal energy creates free electrons and holes in pairs, (Fig. 3) there are precisely as many free electrons as holes, resulting in a zero-total current. This type is not very useful since they are not very good insulators or outstanding conductors. Therefore, intrinsic semiconductors are doped with impurities to become extrinsic semiconductors, which are used in simple components such as diodes, transistors, varistors, photovoltaic cells, photosensitive cells, laser emitter-receivers, and integrated circuits.

1.1.2 Extrinsic Semiconductors

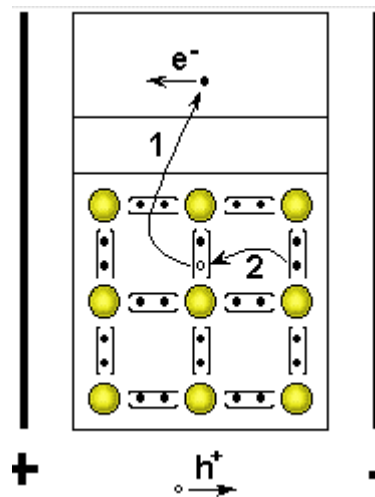


Figure 3. Intrinsic semiconductor diagram

When a small percentage of impurities²⁴, such as trivalent or pentavalent elements, are added to an intrinsic semiconductor, the semiconductor is referred to as extrinsic, and it is said to be doped. Impurities must become a part of the crystalline structure, taking the place of the semiconductor element's corresponding atom, depending on whether it is doped with trivalent or pentavalent elements. Extrinsic semiconductors are classified into two groups due to doping: atoms with an additional electron (n-type for negative, from group V, such as phosphorus) and atoms with one less electron (p-type for positive, from group III, such as boron).

1.1.2.1 n-type Semiconductors

The n-type semiconductor is obtained through the introduction of pentavalent impurities, also known as donors. The most common example of such doping is realized with elements with five valence electrons such as Phosphorus (P), Arsenic (As), or Antimony (Sb). The donor contributes to an excess of electrons, which, since they are unbound, can easily pass through the crystal lattice, enhancing its conductivity. In such a semiconductor, electrons are referred to as "majority carriers," while holes are referred to as "minority carriers." Fig 4. Shows the electrons in the conduction band are represented by “-,” while the holes in the valence band are represented by the “+.” The picture depicts electrons as the majority charge carriers.

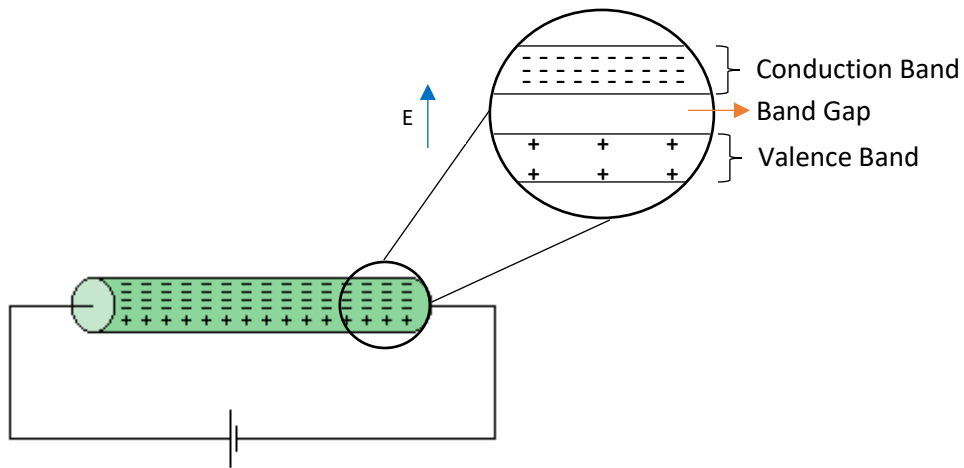


Figure 4. N-type semiconductor and its band structure.

1.1.2.2 p-type Semiconductors

The p-type semiconductor is impurified by trivalent impurities, known as electron acceptors. Boron (B), Indium (In), and Gallium (Ga) can be used as dopants since they possess three valence electrons. Since they lack of the four electrons required to form the four covalent bonds, these atoms would exhibit an electron defect which would induce an atomic defect in the crystal lattice. In this way, holes are produced that allow electrons from outside the crystal lattice to pass through. As a result, holes are the “majority carriers,” while electrons are the “minority carriers.” Fig 5. shows the electrons in the conduction band are represented by “-,” while the holes in the valence band are represented by “+.” The picture reveals that most charge carriers are holes. Although in these two figures it appears that the entire conduction band is filled with electrons, normally only a part is filled with doping.

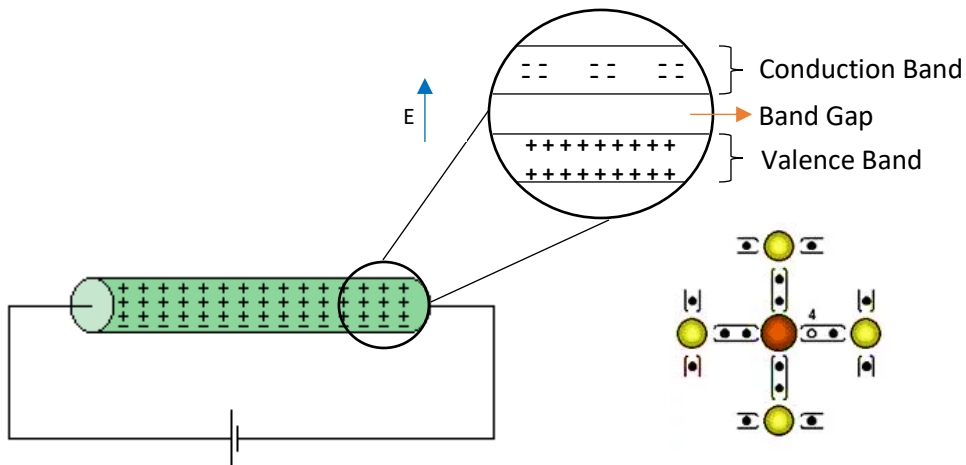


Figure 5. P-type semiconductor diagram and its band structure.

1.1.3 Direct and Indirect Band Gap Semiconductors

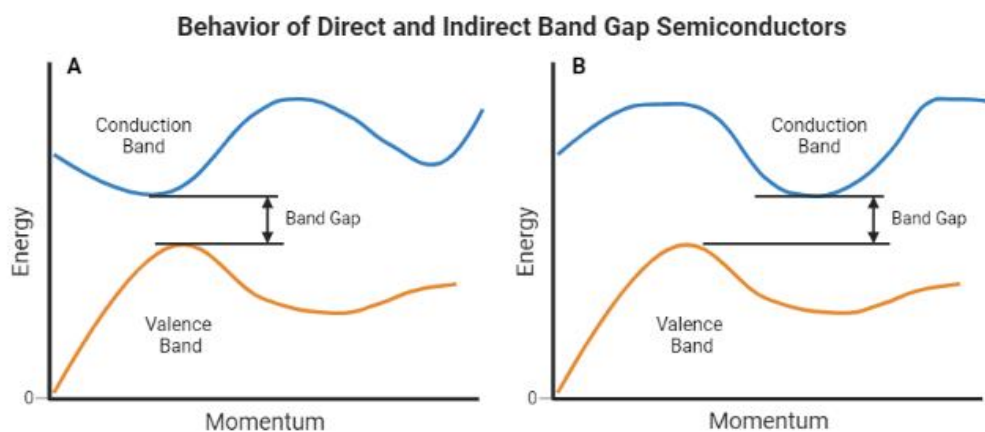
In all cases, the bandgap is just the smallest energy difference between the top of the valence band and the bottom of the conduction band. But the electron momentum of the top of the valence band and the bottom of the conduction band is not always the same. Both direct and indirect behaviors can be observed, as seen in the schematic below (Fig 6).

1.1.3.1 Direct Band Gap Semiconductors

The top of the valence band and the bottom of the conduction band in this type of semiconductor have the same momentum size. In this semiconductor, a photon of energy E_g , where E_g is the band gap energy, will easily create an electron-hole pair because the electron does not need much momentum. Besides, a direct band gap semiconductor has a much more effective recombination mechanism than an indirect band gap semiconductor, which requires intervention of a phonon to complete the process.

1.1.3.2 Indirect Band Gap Semiconductors

In this case, the valence band's maximal energy exists at a different momentum value than the conduction band's minimum energy. Moreover, an electron must also undergo a large shift in momentum in order for a photon of energy E_g to form



an electron-hole pair. This is conceivable, but it necessitates that the electron interferes not only with the photon to gain energy, but also with a phonon, a lattice vibration, to gain or lose momentum.

*Figure 6. Behavior of (A) Direct and (B) Indirect Band Gap Semiconductors.
Created with BioRender.com*

In optics, the distinction between the two is particularly significant. A photon may provide the energy to create an electron-hole pair, as described in the section charge carriers in semiconductors. Gallium arsenide and other direct band gap semiconductors are used to produce optical instruments such as LEDs and semiconductor lasers as a result of these reasons, although silicon, which is an indirect band gap semiconductor, is not.

1.1.4 Heisenberg's principle

The uncertainty principle of Heisenberg is a fundamental principle of quantum mechanics. The uncertainty theory can also be expressed in terms of the momentum and location of a particle. In few words, it goes something like this: if we know exactly where a particle is (the uncertainty of location is small), we know nothing about its momentum (the uncertainty of momentum is large), and vice versa. Other quantities, such as energy and time, have their own versions of the uncertainty principle. Besides, for an unstable atom or nucleus, the relationship holds between the instability in the amount of energy radiated and the uncertainty in the unstable system's lifespan as it transitions to a more stable state²⁵.

1.2 Imaging

Capturing, storing, manipulating, and showing images is referred as imaging. Within digital medicine, imaging focuses on producing photographs of different parts of the human body for diagnostic and treatment purposes. In any medical environment and at all healthcare levels, imaging is essential since its use aids doctors in making more precise diagnoses and treatment decisions. Both diagnosis and care in digital health can be challenging to accomplish with any degree of accuracy without medical imaging. As a result, one of the problems in the biomedical manufacturing is the need for entirely new materials with new properties. Medical imaging covers a wide variety of radiological imaging methods, including X-ray radiography, X-ray computed tomography (CT), fluoroscopy, magnetic resonance imaging (MRI), ultrasonography, or ultrasound, endoscopy, elastography, thermography, among others. Imaging in the medical field often includes measurement and recording techniques that generate data, often depicted as graphs or maps beyond images. Electroencephalography (EEG),

magnetoencephalography (MEG), and electrocardiography (EKG) are examples of these.

Table 2 compiles critical applications for imaging techniques, including their uses.

Table 2. *Most common modalities for various types of imaging tests.*

Test	Method/Process Description and Uses	References
X-Ray	X-ray radiography is a form of radiography that uses X-ray. X-ray computed tomography (CT) is another powerful diagnostic tool providing diverse X-ray absorption densities of tissues with high sensitivity.	26,27
Computed Tomography (CT)	Usually known as a CAT scan (computerized axial tomography). CT has greater spatial and density resolution than other imaging modalities, and it has the potential to provide high-resolution 3D anatomic structure knowledge of tissues based on their differential X-ray absorption ability. Angiography is a type of CT scan.	28–31
Fluoroscopy	Fluoroscopy is based in fluorescence imaging method that uses light to reveal internal different parts and structures of the human body in real-time images, including upper gastrointestinal and barium enema cancer cells.	32,33
Magnetic Resonance Imaging (MRI)	MRI is a noninvasive, nonionizing form of imaging widely used as a clinical diagnostic tool, provides high sensitivity and discrimination, and owns high spatial resolution and excellent soft-tissue contrast. MRI scanning creates 2D photographs of the body and brain.	34–36
Ultrasonography	Also known as medical ultrasonography or ultrasound, it generates photographs of a fetus, internal organs, muscles like the heart; the breast, lungs, tendons, arteries, and veins are also used to make diagnoses.	
Scintigraphy	Scintigraphy is a technique for capturing 2D photographs from the radiation released by injected radioisotopes to locate biological activity areas that may be interestly linked to disease.	
Thermography	Among thermography methods to detect breast tumors through applications are contact thermography, tele-thermography, and dynamic angiothermography.	37,38
Tactile Perception	Tactile imaging allows the creation of images of breasts, the prostate, vagina, pelvic floor, by converting the sense of touch into digital images, as well as myofascial trigger points in muscles.	
Positron Emission Tomography (PET)	PET helps diagnose or treat different pathologies by using the properties of isotopes and energetic particles emitted from radioactive material. I.e., to diagnose specific types of cancer.	39,40

1.2.1 Application

Imaging techniques in the medical field have a wide range of uses, including projection-radiographs to detect bone fractures, pathological changes in the lungs, and diagnosing some forms of colon cancer, mapping of the elastic properties of soft tissue in the body. Similarly, techniques for creating images of the structures of delicate parts of the body

using tomography (CT, PET scanning) and echocardiography, a procedure that allows doctors to examine the heart in-depth, including chamber size, heart rhythm, heart valves, and the pericardium.

Nanotechnology is currently being scrutinized in this context to see how the potential capabilities it represents can be applied to current medical needs^{28,41}. Quantum dots (QDs)-based nanotechnology has been extensively used in bioimaging and research, whose consequence, is becoming one of the most important guiding forces in basic and applied research. Up to date, the use of nanotechnology in bioimaging has been emphasized. Many luminescent QDs were discovered by *in vitro* labeling, including narrow emission, light fluorescence, broad UV excitation, and high photostability. The QDs still has much promise in whole-body imaging⁴².

1.2.1.1 Bioimaging

The processing of images within a biological system at the cellular level is a major challenge in noninvasive biomedical imaging, or well-known as bioimaging. Bioimaging is a key biotechnology process that aims to develop new techniques for imaging specific molecular pathways in living cells or the human body⁴³. There has been an ongoing search in the nanotechnology area for new materials that can be engineered for bioimaging purposes to non-invasively examine biological processes *in vivo* at the cellular and molecular levels. The most important factors that decide the materials used for bioimaging are solid biocompatibility, versatile chemical modification, low cytotoxicity, and superior optical features like photostability, absorption or emission of light in a different way from the near range and low cost, low environmental impact and high stability as advantages. Transition metal dichalcogenides (TMDCs)^{39,44-46}, graphene⁴⁷⁻⁵² and its derivatives (GO-BaGdF5)⁴⁷, and other 2D nanomaterials, for instance, boron nitride^{43,53-56} (BN), graphitic carbon nitride (g-C3N4), and black phosphorus; layered double hydroxides (LDH)⁵⁷⁻⁶⁰, usual organic dyes and polymers⁶¹, rare-earth metals^{40,62-66}, noble metal systems and nanoparticulate systems⁶⁷ are outstanding materials for biological imaging. Additionally, aside from carbon, there are few examples of new materials isolated from elemental allotropes. Some researchers explored new enhancements for the imaging performance of those semiconductor-based nanomaterials⁶⁸⁻⁷¹, such as WS₂^{52,53}, WSe₂, MoSe₂⁷², MoS₂^{52,73-75}, In₂Se₃⁷⁶, TiO₂, TiS₂^{45,77,78}, SnS^{79,80} and GaTe⁸¹. These materials are of recent creation, and their research

status is just growing. Therefore, although they are mentioned, they will not be reviewed in detail in this work.

Nevertheless, some impediments severely limit their practical applications; for instance, graphene is constrained by its zero bandgaps, despite its greater carrier mobility. Its zero bandgaps restrict it from being used as a semiconductor⁸². LDH application is also restricted due to the lack of absorption in the visible range⁸³. Likewise, organic dyes and polymers have low stability among the developed candidates, high price, and unsatisfactory cytotoxicity, i.e. renal toxicity from iodine through computed tomography^{43,84} of rare-earth metals noble metal systems^{43,85,86}. Moreover, MRI is not appropriate for imaging patients with magnetic hardware, and it also does not show any signal for high-density calculus or calcification. On the other hand, to overcome the shortages of inorganic nanomaterials' possible long-term toxicity^{87,88}, developing of a new bioimaging nano agent with good biocompatibility and efficient imaging efficiency is necessary. Several new nanoparticulate CT contrast agents with high atomic number metal elements, such as Au and Bi₂S₃ nanomaterials, have been developed.

Photoacoustic Imaging (PA)

PA imaging is a new and promising non-ionizing and noninvasive imaging modality with high optical contrast, good penetration depth, sensitivity, high-contrast and high spatial resolution (depths up to several centimeters), based on the thermal wave produced by the photosensitizer, used in *in vivo* tumor angiogenesis monitoring, functional brain imaging, blood oxygenation mapping, and skin melanoma detection. PA imaging (PAI) can overcome the drawbacks of ultrasound imaging and optical imaging (i.e., speckle artifacts and limited penetration depth, respectively^{89,90}). It utilizes a modern technology that incorporates both optical imaging^{37,91-94} and ultrasound imaging^{39,45,48,90,92}. Despite the fact that the PA signal originates from the tumor site, its amplitude is low, especially in the early stages. As a result, an efficient exogenous contrast agent for *in vivo* PAI of the tumor site is highly desirable.⁸⁷. Henceforth, the use of inorganic nanomaterials as exogenous agents is intriguing because their unique properties *in vivo* PAI outperform those of organic molecules. These materials guarantee sensitivity, high spatial resolution, and depth-resolved 3D imaging, meaning that they have a bright future *in vivo* bioimaging⁹⁵⁻⁹⁷.

Near-Infrared Region (NIR)

Today's common modalities, such as magnetic resonance or computed tomography imaging, have the advantage of being able to visualize deeply any part of a living organism. However, they are limited to millimeter resolution and therefore cannot be used for surgical guidance. Optical imaging methods have a resolution of 100 nanometers, but they are limited by biological matter's heavy attenuation of visible light, and they have typically been used to image the surface.

Near-infrared, mid-infrared, and far-infrared radiation are the three spectral regions of infrared light. The transparent window for deep tissue penetration is the NIR (700–2,500 nm) zone, where most current photothermal agents absorb light. Since biological tissues scatter and absorb less light at longer wavelengths, near-infrared light can penetrate biological tissues like skin and blood more effectively than visible light^{98,99}. Since near-infrared (NIR) light can penetrate tissues, researchers have investigated NIR absorbing nanomaterials such as metals organic fluorophores, semiconductor quantum dots, rare earth materials, and polymer particles, carbon-based materials, and carbon^{43,45,47–49,93,100–102} nanostructures and their new combine byproducts. They are explored in terms of their physical and chemical properties and their bioconjugation and application.

Fluorescence Imaging

Fluorescence is a property of molecules that allows them to absorb light at one wavelength while emitting light at a longer wavelength¹⁰³. NIR fluorescence emission^{104,105} is commonly favored for *in vivo* fluorescence imaging because deep tissue penetration and a strong signal-to-background ratio are desirable features. Furthermore, two types of fluorescence imaging can be defined: Fluorescence Reflectance Imaging (FRI) and Tomographic Fluorescence Imaging (TFI). For chorioretinal fluorescence angiography, dyes like fluorescein or indocyanine green (ICG) are commonly used^{106,107}. Based on the higher tissue penetration and lower autofluorescence at these wavelengths, various other possible clinical uses of FI with animal and human subjects have been suggested using the NIR of the spectrum. Several fluorescent nanomaterials have been developed to work in the near-infrared, but only a few percentage emitting above 1000 nm have been developed, and none have been approved for clinical use yet. However, recent developments in the design and application of near-infrared fluorescent nanomaterials for biomedical imaging. As compared to conventional organic fluorescein, inorganic quantum dots (QDs) showed significantly improved fluorescent performance

for bioimaging, including tunable wavelength, improved photostability, and high quantum yields. Traditional inorganic QDs, on the other hand, like Cd-based QDs, contain toxic heavy metal atoms, restricting further potential clinical applications⁴⁸.

2.1 Problem Statement

Semiconductors and their brand-new technologies are mainly used in various applications, such as batteries^{108,109}, photodetectors^{75,90,110,111}, photocatalyst,^{112–116} drug delivery^{67,117–119}, sensing devices^{120–122}, electronics, and lasers^{45,123–128}. However, there has not been enough focus on semiconductor promising medical applications¹²⁹ at the nanoscale. To promote the use of semiconductor QDs in the biomedical field, this work summarized SC-based nanostructures' progress in the biomedical field, particularly in the imaging area.

1.4 General and Specific Objectives

1.4.1 General objective

To prepare a review file with related, applicable, and current information on the different studies and methods used to design and improve specific semiconductor-based Nanoparticles for their further use in imaging.

1.4.2 Specific objectives

- i. To summarize the information found in the literature about the description and analysis of the broad field of semiconductor nanoparticles generally.
- ii. To report general details on the methods used to synthesize each semiconductor nanoparticle either by the chemical or the green method.
- iii. To highlight the first main biomedical application and their incidence in such field.

1.5 Overview

This work presents a comprehensive-theoretical assessment of the published literature concerning the recent advances in the synthesis of semiconductor-based nanoparticles in the imaging field. Chapter II provides an insight into the basic definitions and, structures, Chapter III discusses the synthesis and possible experimental routes and sheds light on the properties concerning their focused application, including green chemical synthesis. Chapter IV considers the future directions, suggestions, and discussion regarding the research and emergence in the biomedical field.

Chapter II

2. Semiconductor nanoparticles

Atoms in a semiconductor are from either group IV of the periodic table, or a group combination such as III with V (known as III-V semiconductors) or group II and group VI and so on²⁷.

At the nanoscale, a semiconductor is called a quantum dot (QD). It means the different groups of semiconductors, their binary, tertiary, and other derivative alloys semiconductor materials with a confined size (ranging from 1 to 20 nm)^{33,130} on the nanoscale in three dimensions are referred to as QDs. In 1985, Brus found the first colloidal QDs, which were CdS and ZnS particles¹³¹. Today, there are many different types of particles in this field, with fluorescence properties that can be tuned from visible to far NIR II³⁰. Those exceptional semiconductor nanomaterials have become a famous imaging agent and rank above other fluorescent nanomaterials and traditional dyes¹³²⁻¹³⁵, even their bulk counterparts¹³⁶⁻¹⁴⁰. However, inorganic QDs, on the other hand, also contain poisonous heavy metal atoms (e.g., Cd-based QDs), limiting future therapeutic applications. Nevertheless, to characterize the same substance in nanoparticulate form, a risk assessment for bulk materials is insufficient¹⁴¹, so it still represents a challenge. Hence, most QDs used in analytical applications are made as core/shell structures, in which the nanocrystal's core is coated with different semiconductor material to preserve and strengthen its properties and they are functionalized and encapsulated¹⁴². Non-Cd QDs and NIR-II window QDs, such as InAs/InP/ZnSe Core/Shell/Shell QDs, are part of the latest generation of QDs^{42,143} whose start took place from 2011 approximately. As a result, the toxicity of heavy metal-based QDs is minimized by covering the center of the QDs with polymeric shell coatings that mechanically inhibit (in a partial way) heavy metal ions from leaching out and increase stability¹⁴⁴. One more advantage is the obtention of multiplex emission with single light source excitation with minimal spectral overlap. The outstanding optoelectronic properties of QDs include high quantum yield (QY), which covers from 1–8% in the visible, and 2–7% in the NIR¹⁴⁵, size-dependent,

narrow light emission, broad absorption spectra (spectral windows spanning from the UV region), long fluorescence lifetime, photo-stability, simultaneous excitation of multiple QDs by a single light source provoking a massive stoke shift, and resistance to photobleaching^{146–148}.

Because of their intriguing optical and electronic properties, semiconductor nanoparticles have gotten much attention. In particular, quantum dots can be used to refer to traditional compound semiconductor nanoparticles. Since the groups on the surface of QDs can bind to essential proteins abundant in cell nuclei, they can be used for direct cell imaging. As fig. 6 shows, biomolecular tracking of cells, cellular imaging, and tissue staining are all done *in vitro*. QD biodistribution, vascular imaging, QD mapping, and tumor imaging are all done *in vivo*.

The group categories of QDs are listed on annexes; nonetheless, surface modifications, photoluminescence properties, emission ranges, and imaging applications are all mentioned in the following paragraphs within this work.

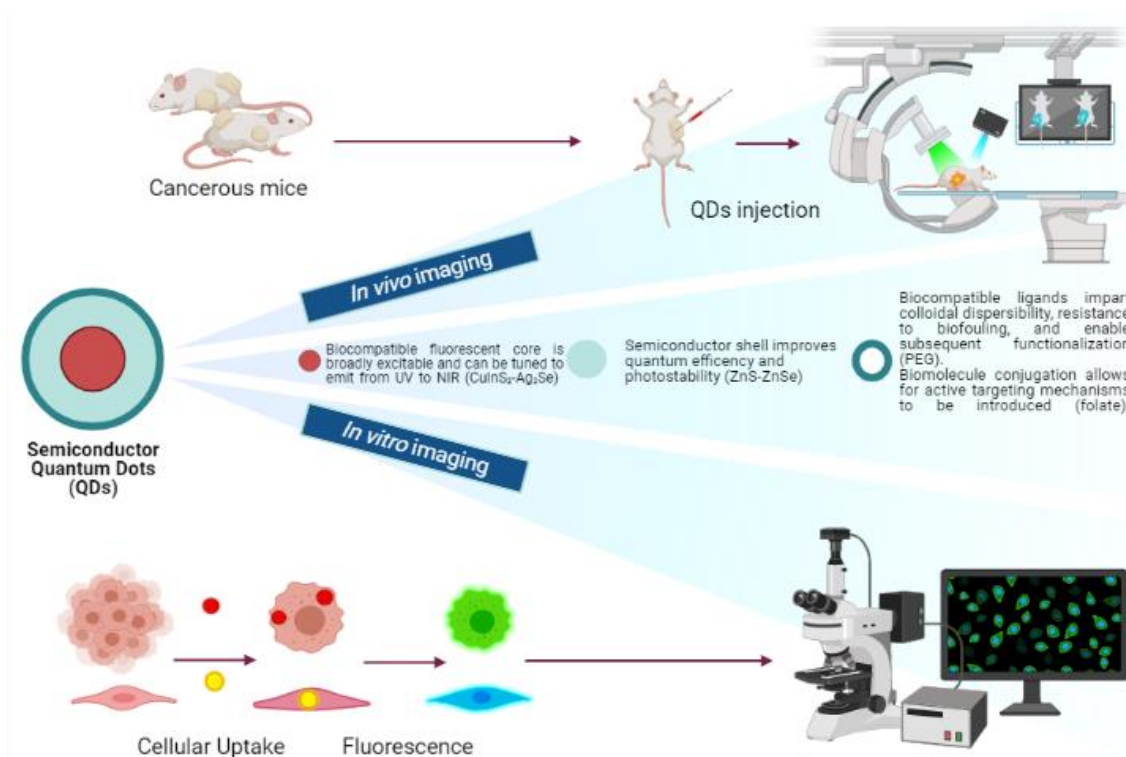


Figure 7. Schematic of typical QDs structure containing a fluorescent core, wide bandgap semiconductor shell, surface ligands, and their and QDs imaging systems.

The figure was adapted from^[148]. Created with BioRender.com

2.1 IV Group

Group-IV QDs have recently gained popularity as a non-toxic alternative to traditional II-VI and IV-VI QDs that contain toxic elements like mercury. Within this group, a semiconductor can either be of a single element, such as Si or Ge; a compound, such as SiGe, or an alloy, such as $\text{Si}_x\text{Ge}_{(1-x)}$ or $\text{Al}_x\text{Ga}_{(1-x)}$, where x represents certain fraction of the element and varies from 0 to 1.

		IIIA	IVA	VA	VIA	VIIA
		⁵ B	⁶ C	⁷ N	⁸ O	⁹ F
		¹³ Al	¹⁴ Si	¹⁵ P	¹⁶ S	¹⁷ Cl
²⁹ Cu	³⁰ Zn	³¹ Ga	³² Ge	³³ As	³⁴ Se	³⁵ Br
⁴⁷ Ag	⁴⁸ Cd	⁴⁹ In	⁵⁰ Sn	⁵¹ Sb	⁵² Te	⁵³ I
⁷⁹ Au	⁸⁰ Hg	⁸¹ Tl	⁸² Pb	⁸³ Bi	⁸⁴ Po	⁸⁵ At

Figure 8. Semiconductors from group IV of the periodic table.

2.1.1 Carbon Dots (CDs)

Regarding this unique type of QD that only has one element: Carbon Dots (CDs), there is a lot of scientific literature^{149–153}. Among CDs, properties are good photostability and biocompatibility, good absorption between 600 and 900 nm, excellent water solubility, low cytotoxicity, a narrow spectral emission, NIR emission for *in vivo* imaging, a high PL QY of 16.8%, and a favored uptake of the two-photon fluorescence bioimaging features. By 850 nm light from a femtosecond pulsed laser, the red-emitting CD (maximum emission of 683 nm) may be excited. These CDs could be used for deep tissue two-photon excitation bio-imaging and as a carrier for drugs that cannot be injected directly into living cells¹⁵⁴.

2.1.1. Application

Fluorescence Imaging: Lan et al.¹⁵⁵ used a hydrothermal process to prepare CDs co-doped with S, Se. Thus, NIR emissions of the CDs, with PL bands peaking at 731 and 820 nm and photothermal conversion efficiency of 58.2% were obtained. The CDs have a high enough two-photon absorption cross-section to emit NIR light. A CD appear to be a useful phototheranostic agent for two-photon excitation fluorescence imaging and photothermal therapy of *in vitro* and *in vivo* studies on cancer cells. Li et al^{156,157}. demonstrated that surface-modified CDs could absorb light and emit NIR light. CDs in

dimethyl sulfoxide (DMSO) have a NIR-I absorption band at 715 nm and a NIR emission band at 760 nm, along with a PL QY reaching 10% under NIR excitation. In order to achieve *in vivo* fluorescence imaging, CDs require both NIR excitation and emission. Under the excitation of light peaking in the NIR-II window, two-photon and three-photon mediated fluorescence have been observed in DMSO. For *in vivo* NIR fluorescence imaging, CDs modified with polyvinyl pyrrolidone (PVP) is placed in the stomach of a living mouse. This is the first method for efficiently producing CDs with a NIR absorption band and NIR emissive CDs with either one-photon excitation in a NIR-I or multiphoton excitation in a NIR-II window used in NIR fluorescence imaging.

2.1.2 Germanium (Ge)

Because of its indirect bandgap character, Ge bulk crystal is a typical indirect bandgap semiconductor with a narrow bandgap of 0.7 eV at room temperature and poor optical efficiency. The energy structure is altered by carrier confinement in a Ge NP with a diameter smaller than the bulk exciton Bohr radius (11.6 nm), The highly tunable quantum confinement effects in Ge QDs are demonstrated by the NIR absorption with 1.6-0.70 eV) and corresponding band-edge emission. The relaxation of the k-selection rule due to the Heisenberg uncertainty relation allows for the overlapped wave functions of spatially confined carriers, resulting in zero-phonon optical interband transitions for recombination. Controlling the size and structure of QDs results in emission tunability across the entire visible wavelength spectrum¹⁵⁸, i.e. yellow emitting Ge QDs. In comparison, Karatutlu A et al.¹⁵⁹ record fluorescence colors in the near-infrared wavelength range. A biological window of 900–1600 nm was used to achieve continuous tunability. However, for fluorescence biomarkers, the emission QY is still extremely low (5%).

2.1.3 Silicon (Si)

Silicon is a metalloid chemical element that belongs to the periodic table's group IV A. It comes in two forms: amorphous and crystallized. The amorphous form is a brownish powder that is more active than the crystalline form, grayish-blue octahedra with a metallic luster. Usually, Si forms are found in silicon dioxide and complex silicates. There are nine isotopes of silicon, with mass numbers ranging from 25 to 33. Si-28 is the most abundant isotope, with a 92.23 percent abundance, followed by Si-29 and Si-30. Some of them are stable through the time, with the majority of the isotopes making up a tiny percentage. Si-32 is a radioactive isotope formed as argon decays. Si energy bandgap ranges from 1.00 to 1.25 eV²⁷. For the first time, Wang et al. ¹⁶⁰ in 2004 announced the

bio-medical use of Si QDs as a fluorescence marker of DNA. By that time, some contributions to this area of study have been made for high hydrophilicity and biocompatibility¹⁶¹.

Silicon quantum dots (SiQDs)

The bulk crystalline silicon (Si) is classified as an indirect bandgap semiconductor with a bandgap of 1.1 eV at room temperature. The electronic structure of Si QD retains its indirect bandgap character, as is well understood. The uncertainty principle predicts the presence of PL peaks tailing on the low energy side. This tailing continues until Si reaches 1.1 eV, which is the same as the bulk bandgap value for crystalline Si. Chandra et al.¹⁶² created a water-generated Si QD modified for 2-photon excitation and used it to provide indisputable proof of NIR-NIR excitation-emission imaging for the first time.

Furthermore, even after the surface ligands are replaced, the size-dependency of PL peak energy is observed. An improvement in the radiative recombination rate¹⁶³, a dramatic reduction of the non-radiative channels^{164,165}, or a bandgap modulation from indirect to direct transitions¹⁶⁶ are thought to be the causes of a high PL QY. This form of PL QY enhancement has been recorded for alkyl terminated QDs with size-dependent PL bands, which encourages the creation of QD-based optoelectronics devices^{167,168}. Furthermore, Si QDs are nontoxic, have a long PL lifetime on a μ second scale, are light, and emit fluorescence from UV to NIR wavelength range¹⁶⁹⁻¹⁷³. Non-thermal Plasma or thermal disproportionation of hydrogen silsesquioxane ($\text{HSiO}_{1.5}$), accompanied by hydrofluoric etching to free the Si QDs from the oxide matrix, have been used to prepare Si QDs¹⁷⁴. In the majority of studies. Boron, phosphorus, and transition metal impurity doping into the diamond cubic Si lattice have also been accomplished^{175,176}. Sakiyama et al.¹⁷⁷ recently produced a long-lived colloidal silicon QD luminescence for time-gated fluorescence imaging in the second NIR window in biological tissue.

Due to their ability to exhibit size-dependent luminescence in the red to near-infrared (NIR) wavelength (range in quantum size effects^{127,178-180}), and to fluoresce blue and red light (ranging in size from 1 to 10 nm), SiQDs are semiconductor nanoparticles that have great potential as optoelectronic devices and fluorescent biological marking agents¹⁸¹. Additionally, since Si tends to be oxidized, most currently synthesized SiQDs have blue fluorescence properties¹⁸². The fluorescence intensity, toxicity, and biocompatibility are all issues that must be addressed before they can be used in biological imaging. Another concerning aspect is the SiQDs low aqueous dispersibility. Regarding their toxicity and

biocompatibility, significant progress has been made in producing hydrophilic SiQDs, involving photochemistry and microwave-assisted synthesis of water-dispersible SiQDs¹⁸³, as well as for cellular probes. Surface modification is another way to change the solubility of SiQDs in water^{184,185}. Another factor that can help SiQDs stay stable is encapsulation, which is explored using biocompatible polymer matrices for bioimaging^{181,186}.

2.1.1.1 Application

Fluorescence Imaging: Si NCs that meet all three requirements for an idealized Si NC bioimaging agent, namely, NCs with tunable excitation, emission, and quantum yields, as well as NCs that are stable in water/biological environments. This is accomplished by employing metal dopants and making precise adjustments of their concentrations¹⁸⁷. Besides, when these SiQDs are used for cell imaging, the organism's cells and tissues have an apparent blue background fluorescence, making it challenging to discern signals from background signals. As a result, one of the problems that need to be resolved is the synthesis of red-emitting SiQDs. Chen et al.¹⁸⁸ made advances in SIQDs: the fluorescence strength of SiQDs is increased by glutamate, and their dispersion is improved by PVP. So, their fluorescence has a high photoluminescent quantum yield of up to 23.22% and no visible quenching in the room atmosphere, even in storage.

Moreover, The CT26, MB49, and 4T1 cell lines were used to test the cytotoxicity of the two-component-modified SiQDs, suggesting that the glutamate/PVP-modified SiQDs have no toxicity *in vitro*. In Fujii et al.¹⁸⁹ work, the SiQDs have an amorphous shell that is strongly B and P co-doped, and the shell induces negative potential on the surface, which prevents their agglomeration in polar solvents. Regulated agglomeration of Si QDs occurs when toluene is added to the methanol solution, resulting in spherical superparticles about 100 nm in diameter with a narrow size dispersion. The excellent cytotoxicity of Si QDs onto osteoblasts, monocytes, macrophages, and mesenchymal stromal cells has been addressed¹⁹⁰.

2.2 III-V Group

Among the II-VI, III-V, and IV-VI semiconductor QDs, high-quality InAs, InP QDs are likely the best candidate for NIR-light emitters ($\lambda_{em} = 700\text{--}1400\text{ nm}$).

Table 3. Updated methods of Si QDs synthesis for bioimaging. A comparison of synthetic conditions for preparing Si nanostructures with different precursors, solvents, reactions, and conditions for the green chemical method.

Morphology	Synthesis/Obtainment Method	Precursors/Initiators	Conjugated/Anchored Chemical/Ligand/Solvent Functionalization	Advantage/Improvement	Specific imaging technique	Reference/Year
Silicon Quantum Dots (SiQDs)	Electrochemical Etching method	Inorganic Si QDs	Methanol solution of boron (B) and phosphorus (P), Toluene, aqueous HF with H ₂ O ₂ 106 or HNO ₃ and different additives like polyoxometalates	Electrochemical enhancement	Fluorescence	181 2020
	Electrochemical etching method, ultrasonic treatment. Surface modification	p-type Si wafer	Glutamate and PVP, Hydrofluoric acid (HF), hydrogen peroxide, ethanol and n-hexane	Increased fluorescence intensity and enhanced solubility-dispersion in water, low toxicity.	Fluorescence	191 2019

		IIIA	IVA	VA	VIA	VIIA
		⁵ B	⁶ C	⁷ N	⁸ O	⁹ F
IB	IIB	¹³ Al	¹⁴ Si	¹⁵ P	¹⁶ S	¹⁷ Cl
²⁹ Cu	³⁰ Zn	³¹ Ga	³² Ge	³³ As	³⁴ Se	³⁵ Br
⁴⁷ Ag	⁴⁸ Cd	⁴⁹ In	⁵⁰ Sn	⁵¹ Sb	⁵² Te	⁵³ I
⁷⁹ Au	⁸⁰ Hg	⁸¹ Tl	⁸² Pb	⁸³ Bi	⁸⁴ Po	⁸⁵ At

Figure 9. Semiconductors from either elements or combinations of group III and group V (called III-V semiconductors).

A focusing of size distribution was used to create InAs QDs with NIR-emitting properties. Some structures Cu-dopant emissions are: InP/ZnSe core/shell QDs, water-soluble InAs (ZnCdS) QDs, InAs (ZnCdS) QDs. InP QDs. Core-shell QDs with bright (up to 90% PL QY), stable, and narrow NIR-PL spectra can be made in one pot, ideal for in vivo biomedical imaging. By epitaxially growing of ZnSe and InP, Cu-doped QDs were successfully synthesized. Bruns et al.¹⁹² identified InAs-based core-shell and core-shell-shell QDs emitting in the short-wavelength infrared region (SWIR) as a versatile class of materials for functional biological imaging. Indium-based QDs, such as InP, are stated to be nontoxic in the group III-V class, and their quantum yield can be increased from 5% up to 57 % in an aqueous environment through controlled synthesis¹⁹³.

2.2.2 Boron (B)

Boron is a trivalent, semiconductor, metalloid chemical element that exists abundantly in the mineral borax. B belongs to group IIIB of the periodic table. Because of their higher electronegativity, boron atoms are electronegativity attracted by nitrogen atoms¹⁹⁴, resulting in creating an anionic character. Boron can exist in allotropes forms, from 0D to 3D, and has a wide range of properties, including metal, semimetal, and nonmetal¹⁹⁵. Boron allotropes come in two forms: amorphous and metallic. Amorphous boron is a brown powder, while metallic boron is black. The semiconductor compounds that can be formed between boron and VA elements are Boron Nitride (BN), Boron Phosphide (BP), and Boron Arsenide (BAs). Borophene, or ultrathin boron nanosheets (B NSs), is a newcomer to this group. Among its characteristics are its structural polymorphism, tunable band structure, and excellent photoluminescence^{196–199}.

Boron Nitride (BN)

BN is a fluorescent wide-bandgap semiconductor nanomaterial²⁰⁰, and it is made up of the same amount of boron and nitrogen atoms. This material was previously thought to be only synthetic, until it has been found in nature in 2009²⁰¹. They come in three crystalline forms: graphite-like hexagonal BN (h-BN), diamond-like cubic BN (c-BN)²⁰², and wurtzite (w-BN), all of which are isoelectronic to the analogous structured carbon lattices. The fabrication processes of various BN derivatives, hetero and porous structures are defined in detail using various functionalization methods, including physical and chemical routes. Various synthesis studies on hBN have shown that it can exist in various dimensionalities, such as quantum dots^{54,203}, nanoribbons, and nanoscrolls^{55,204–206}, 2D nanosheets^{74,207–209}, nanotubes^{55,202,207,210–212}, nanoflakes^{94,204,207} as well as several of its nanomaterial equivalents, ie. Foams²¹³.

Under standard conditions, h-BN^{51,204,207,214,215} is the most stable BN among them. hBN is part of the 2D materials which exhibits excellent chemical and physical properties. Since h-BN has a layered structure like graphite, it could be considered as its analog. A two-dimensional (2D) layer, strong B–N covalent bonds bind alternating B and N atoms together, whereas weak van der Waals forces hold the 2D layers together⁵⁵.

Furthermore, high water solubility, excellent biocompatibility, tunable surface affinities, low dielectric constant, high-temperature stability, high corrosion resistance, high thermal conductivity, good processibility²¹⁴, flexible band gaps, and other novel properties of functionalized BN materials have ensured large applications in the biomedical, electronic, composite, and environmental fields, In fact, in ultraviolet optoelectronics and nanoelectronics, boron nitride is gaining popularity due to the mentioned above features. Furthermore, the photonics and plasmonic properties of h-BN are intriguing. However, the application of h-BN is also limited by their insulating properties and their lack of absorption in the visible region. Among the synthesis methods are: chemical vapor deposition (CVD)^{216–219}, laser ablation²²⁰, ball milling, ultrasonication^{206,207}, plasma jet, and carbon use nanotubes as templates are some of the techniques used. Besides, mechanical spinning²⁰⁴ as top-down methods and another method such as gradient method²⁰⁵.

To date, even though several new synthetic routes are available, CVD is the best one since it allows scalability, good quality, and control over size, yet remains the need of costly

equipment and substrate-based method. Boron Oxide CVD (BOCVD)²¹⁸ technique was recently adopted. Unlike vapor-based approaches, liquid-phase exfoliation (LPE) has recently been recognized as a viable technique for fabricating 2D nanomaterials, as it combines the benefits of ease of use, high yield, low cost, and environmental friendliness.

2.2.1.1 Application

In bioimaging, functionalized h-BN nanosheets, also known as white graphene, are used due to their extremely low cytotoxicity, excellent water dispersion, low fluorescence quenching,¹⁹⁴ chemical resistance, high stability and mechanical strength²⁰⁷, as well as, electronic properties such as tunable band gap and thermal stability. Many other important electrical, optical, and chemical properties are conferred on h-BN by its special structural features. The reduced electron delocalization in BN π -bonds, for example, results in a large bandgap ($> 5\text{eV}$) and an electrically insulating nature¹⁹⁴. Moreover, they may be used as biosensors because of their cell-penetrating effect and intense fluorescence.

Fluorescence Imaging: In 2013, Peng et al.⁵¹ showed that h-BN combined with graphene quantum dots could be used as a green fluorescent nanoprobe for cellular imaging and showed improved water solubility, stability, and low cytotoxicity On HeLa cells. However, both molecules and QDs tend to bleach and blink. Therefore, by embedding the molecules in a suitable crystalline matrix or encapsulating the QDs in an engineered higher bandgap shell, the blinking and bleaching can be minimized. To face that limitation, Palombo et al.²¹⁵ proposed the synthesis to make hBN-defects that are optically stable throughout the entire flake via argon plasma etching and subsequent high-temperature annealing. The entire structure released a wide-range emission (covering the wavelength spectrum from 550 to 700nm). Thus, increase the number of emitters in the exfoliated hBN-flakes and the density of tightly packed emitters allow to obtain photoluminescence. For their part, Ma et al.⁴³ worked using liquid-phase exfoliation along with both probe and water bath sonication. So, as a result, they obtained BN structures with strong blue fluorescence, high photostability, good biocompatibility, and low cytotoxicity. The most important aspect of the latter is its biocompatibility when analyzed in HeLa and Huh-7 cancer cells.

Another hurdle is the superhydrophobic nature and strong aggregation propensity in aqueous media. Hence, to make BN nanotubes more dispersible in aqueous media, Kalay

et al.²¹⁰ produced BNNTs and after covalently grafted with polymer brushes via polymerization, specifically brushes made of polystyrene or poly(glycidyl methacrylate) polymer were used to covalently modify the mentioned structures, whose intense green fluorescence is emitted at 520 nm. Because of its low toxicity, human normal prostate epithelium (PNT1A) and human prostate cancer cell lines (DU145) readily accept the functionalized BNNTs, making them suitable for further testing in cellular imaging applications. The hybrid structure formed could be used as “smart” surfaces, nano transducers, and nanocarriers in addition to cellular imaging. Sosnik⁵⁴ et al. synthesized BNQDs started using a solvothermal process under pressure from boron nitride nanoparticles in N,N-dimethylformamide (DMF). Those BNQDs have a quantum yield of $21.75 \pm 0.02\%$. The final BNQDs (20% w/w) is encapsulated inside poly (ethylene glycol)-b-poly(epsilon-caprolactone) nanoparticles by a nanoprecipitation process, resulting in hybrid nanocomposite particles with significantly stronger photoluminescence than their free counterparts, and full dispersibility in water.

2.3 II-VI Group

Most typical II-VI quantum dots can only be excited by light with a wavelength of less than 600 nm, limiting their applications²²¹. Therefore, CdTe and HgTe QDs are most widely used in the near-infrared region. Yet, there are another some structures like CdTe_xSe_{1-x}/ZnS alloy, alloyed CdTe_{1-x}Se_x/CdS NIR QDs²²², alloyed CdHgTe QDs²²³ being part of this group.

2.3.1 Cadmium Telluride CdTe

Gadolinium-functionalized CdHgTe/ZnS core/shell QDs, cyclic arginine-glycine-aspartic acid conjugated micelle-encapsulated NIR CdTe/ZnSe QDs²²⁴, and CdTe/CdSe QDs²²⁵ are suitable fluorescent probes in the imaging of living animals and used for *in vivo* fluorescence and magnetic resonance imaging, as highly luminescent probes²²⁶.

Table 4. Updated methods of BN synthesis for bioimaging. A comparison of synthetic conditions for preparing h-BN nanostructures with different precursors, solvents, reactions, and conditions for the green chemical method.

Morphology	Synthesis/Obtainment Method	Precursors/Initiators	Conjugated/Anchored Chemical/Ligand/Solvent Functionalization	Advantage/Improvement	Specific imaging technique	Reference/Year
Boron Nitride Quantum Dots (BNQDs)	Liquid exfoliation–solvothermal process	BN NPs	Poly (ethylene glycol)- <i>b</i> -poly(epsilon-caprolactone) nanoparticles <i>N, N</i> -dimethylformamide	Stronger photoluminescence, <i>in vitro</i> , optimal cell compatibility, and bioimaging features, complete dispersibility in water.	Fluorescence Imaging	[54] 2021
Boron nitride nanoscrolls (BNs)	Liquid exfoliation, micromechanical exfoliation.	BN powder	<i>o</i> -dichlorobenzene (ODCB) lithocholic acid	Composite with increased stability, enhanced magnetization, and high surface-area-to-volume ratios.	Fluorescence Imaging	[55,206] 2018 2019
	Ultrasonication	Bulk BN	NMP	High-quality BNS with excellent stability, high thermal conductivity		
BN nanotubes- BN nanoflakes	copper catalytic approach, post-synthesis ultrasonication	Boron oxide (B ₂ O ₃), Urea (NH ₂ CONH ₂)	Boric acid (H ₃ BO ₃), copper sulfate pentahydrate, ethanol, and ammonia gas. Tungsten substrate. Nanoantenna	Easy method, good yield and fluorescence properties, bioimaging agent for cancer cells	Fluorescence Imaging	[94,207,214] 2018 2019
	Argon plasma etching-high temperature annealing	h-BN-flakes		Optically stable h-BN flakes,		215 2020
	CVD	Colemanite and Fe ₂ O ₃	4M HCl, HNO ₃ Copolymer brushes (poly (acrylic acid- <i>co</i> -fluorescein acrylate) – P(AA- <i>co</i> -FA)), PEG, pyridine and other organic solvents	pH-Switchable, fluorescent, hybrid material, water-dispersible, and it has a high dispersibility in a wide range of organic solvents, two-step process, intense green fluorescence emission	Fluorescent Imaging	210 2019
Ultrathin Boron Nanosheets (BNSs)	Modified liquid-phase exfoliation	Bulk Boron powder	None	Good structural integrity, strong blue fluorescence, high photostability, good biocompatibility and low cytotoxicity.	Fluorescence Cellular Bioimaging	43 2020

2.3.2 Mercury Chalcogenides

HgTe, HgSe, and HgS have narrow or negative band gaps that led themselves to infrared applications in bulk form. HgTe has a room temperature band gap of -0.32 eV to -0.15 eV and is often referred to as a zero-band gap material. Regarding mercury telluride (HgTe), Geiregat et al.²²⁷ recently demonstrated that HgTe QDs have size-tunable emission all over the NIR window at thresholds unparalleled by any other QDs previously studied. As synthesis improves, more records of HgSe and HgS emerge.

		IIA	IVA	VA	VIA	VIIA
		⁵ B	⁶ C	⁷ N	⁸ O	⁹ F
	IIB	¹³ Al	¹⁴ Si	¹⁵ P	¹⁶ S	¹⁷ Cl
²⁹ Cu	³⁰ Zn	³¹ Ga	³² Ge	³³ As	³⁴ Se	³⁵ Br
⁴⁷ Ag	⁴⁸ Cd	⁴⁹ In	⁵⁰ Sn	⁵¹ Sb	⁵² Te	⁵³ I
⁷⁹ Au	⁸⁰ Hg	⁸¹ Tl	⁸² Pb	⁸³ Bi	⁸⁴ Po	⁸⁵ At

Figure 10. Semiconductors from either elements or combinations of group II B and group VI A (called II-VI semiconductors).

2.3.1.1 Application

Cell imaging: He et al. were the first to publish a simple one-step microwave synthesis of water-soluble CdTe QDs for cell imaging. After conjugation with protein molecules, the water-dispersed NIR CdTe QDs with an emission wavelength of 700–800 nm are used for *in vivo* tumor targeting and *in vitro* imaging for the first time²²⁸. However, more recently, Chen et al.²²⁹, developed a one-pot aqueous synthesis of glutathione (GSH) binding CdTe quantum dots (QDs) with a QY of 49%, and their emission ranges from 520 to 620 nm, depending on their size. On HeLa cells, the bioimaging efficiency of the GSH-capped CdTe QDs is further assessed. Besides, Liu et al.²³⁰ recently produced NIR emitting CdHgTe/CdS/CdZnS QDs and coated them with three separate thiol ligands, 3-MPA, TGA, and N-acetyl-L-cysteine (NAC). The *in vivo* toxicity testing on mice revealed no adverse effects.

Fluorescence Imaging: MPA-stabilized NIR-emitting CdTe/CdS QDs are used to develop a low-detection-limit fluorescence sensor for Cu²⁺, which was used for bioimaging in HeLa cells and Kunming mice. The accumulation of QDs caused by the competitive binding of MPA on the surfaces of NIR QDs and the Cu²⁺ present in the

solution caused the quenching effects. Because of the suitable wavelength spectrum of emission radiation, *in vitro* imaging of HeLa cells and *in vivo* imaging of Kunming mice showed that these NIR QDs are suitable for high-resolution imaging of biological tissues²³¹. One crucial factor was reported by Qu et al.²³². MPA-capped CdTe QDs (50 mg/L) cause irregular oogenesis and reproductive toxicity by disrupting germline cell proliferation and differentiation, disrupting the complex equilibrium between mitosis and meiosis, and inhibiting mediated toxicity mechanisms and mediated defense mechanisms at a risk exposure, also, CdTe induces DNA damage in exposed mouse microglial cells (BV-2 cellular line)²³³. In Guifen²³⁴ et al.'s work, CdTe QDs and doxorubicin (Dox) were used to build a multifunctional DNA nanocage. It was used to detect human 8-oxoG DNA glycosylase 1 (hOGG1) fluorometrically using an exonuclease-assisted cycling amplification technique. The nanocage becomes both a flexible probe for fluorescence imaging of cancer cells, and a drug delivery system as it is filled with the cancer drug (Dox). Dox fluorescence is switched off until it is inserted into the DNA nanocage. The Dox is released, and its fluorescence (measured at excitation or emission wavelengths from 480 to 560 nm) is turned on once the DNA nanocage reaches the MCF-7 cells.

2.4 I-VI Group

The semiconductive materials used to generate them, such as Cadmium, Tellurium, Selenium, are nondegradable. Silver selenide (Ag_2Se), also known as naumannite, is a semiconductor compound that is only present as a mineral in nature. It is an I-VI complex with an 1.2–1.8 eV optical band gap²³⁵. Because of its many implementations, including electronics and the biomedical field^{236,237}, Ag_2Se is one of the most commonly studied chalcogenide nanomaterials among semiconductor nanomaterials. By cation exchange between visible emitting CdS QDs and Ag^+ ions in aqueous solution, Gui et al.²³⁸ reported a simple synthesis of Ag_2S QDs with size-dependent PL bands peaking in the NIR-II region, those Ag_2S QDs had only a tiny impact on the development of reactive oxygen species, suggesting their low cytotoxicity. Alternatively, Ag_2Te QDs and $\text{Ag}_2\text{Te}/\text{ZnS}$ core/shell QDs were also presented, registering in the NIR-II window a maximum emission around 900–1300 nm. Some tertiary and quaternary nano compounds of this group are AgInS_2 , quaternary AgZnInS , $\text{AgInS}_2/\text{ZnS}$, and $\text{AgZnInS}/\text{ZnS}$ ²³⁹. These QDs are extremely small (7.6 nm) and non-toxic to cells, making them ideal for optical bioimaging. After intravenous injection, Tang et al.²³⁶ investigated the blood clearance,

distribution, transformation, excretion, and toxicity of such QDs modified with polyethylene glycol (PEG) in mice. The PEGylated Ag₂Se QDs accumulate in the spleen and liver but are almost entirely transformed into its metabolites and cleared after one day. After all, the PEGylated Ag₂Se QDs show low toxicity, high performance, and proper biosafety. Hydrophilic Ag₂S QDs hold great potential for *in vivo* imaging. Javidi et al.²⁴⁰ performed cytotoxicity experiments on human A549 and Hep G2 cell lines. The QDs showed no significant toxicity in the cytotoxicity test. The water-soluble Ag₂S QDs acts inside the mice body with excellent brightness, according to *in vivo* imaging. These QDs can be used as *in vivo* or as diagnostic NIR bio-imaging probes. The photostability and *in vitro* experiment revealed low cytotoxicity and extremely promising clinical diagnostic applications. Nucleation and growth of Ag₂Se QDs with tunable PL bands peaking in the NIR-II window (max emission of 1000–1400 nm) were achieved using 1-octanethiol, a soft Lewis base, as a ligand.

Ge et al.²⁴¹ investigated the biodistribution and removal of NIR ultra-small Ag₂Se QDs in mice. The bio-distribution fluorescent images of Ag₂Se QDs in mouse organs and inductively coupled plasma mass spectrometry (ICP-MS) studies indicated that the Ag₂Se QDs could be removed quickly from the mice body, usually through renal excretion without accumulating. The Ag₂Se QDs do not cause significant toxicity in the *in vivo* setting, according to pathological, biochemical, and body weight results.

Gui et al.²⁴² demonstrated a simple aqueous synthesis of Ag₂S QDs (2.6–3.7 nm) with bright and tunable PL emission in a wide range from red to NIR-II (emission range from 687 to 1096 nm). As a new theranostic agent, Duman et al. developed the aqueous synthesis of cationic, NIR-emitting Ag₂S QDs, with an emission from 810 to 840 nm with a mixed coating of MPA and Polyethylenimine²⁴³.

Shi et al.²⁴⁴ used ODE–Se as the Se precursor to make high-quality, NIR-emitting Ag₂Se QDs with distinct absorption features and high PL QYs. Using Au nanostructures formed by colloidal lithography, Theodorou et al.²⁴⁵ demonstrated a substantial increase in PL intensity in the NIR-II region for Ag₂S QDs. Chen et al.²⁴⁶ recently analyzed and explored using fluorescent nanoprobes to monitor transplanted stem cells in the first and second biological windows.

2.5 I-III-VI Group

Due to their low toxicity, researchers have recently focused on I-III-VI group semiconductor NPs of Cu or Ag-based materials, such as CuInS_2 , $\text{Cu}(\text{In}, \text{Ga})\text{Se}_2$, i.e., ternary CuInS_2 QDs; AgInS_2 ²⁴⁷ or Zn–In–S QDs. Mao et al. produced NIR-emitting $\text{AgInS}_2/\text{ZnS}$ QDs by heating an Ag/In/Zn/S solution to 165 °C. The formation of NIR emitting QDs was influenced by zinc concentration and temperature rise. Zinc allows $\text{AgInS}_2/\text{ZnS}$ NCs to develop at high temperatures without aggregation and suppresses defects, increasing the PL strength of $\text{AgInS}_2/\text{ZnS}$ QDs. The $\text{AgInS}_2/\text{ZnS}$ NCs' NIR emitting properties make them potentially attractive for bio-imaging applications²⁴⁸. For *in vivo* imaging experiments, Xi et al.²⁴⁹ demonstrated a one-pot synthesis of water-soluble, NIR-emitting CuInS_2 QDs using RNase A; this result confirms that they could be a good candidate for biomedical applications, particularly in the gastrointestinal system. Water-dispersible AgInS_2 QDs with bright NIR emission was demonstrated by Tan et al.²⁵⁰, where a capping ligand for AgInS_2 QDs was synthesized from a form of multidentate polymer. The AgInS_2 QDs with the multidentate polymer capping are luminescent in the NIR window and have excellent photostability; they are also stable in various media and have low cytotoxicity. Mice photoluminescence imaging demonstrates that AgInS_2 QDs with a multidentate polymer capping can be used for *in vivo* imaging. These near-infrared fluorescent QDs have much biomedical potential. For cancer cell staining, Fahmi et al.²⁵¹ rendered water-soluble $\text{AgInS}_2\text{-ZnS}$ QDs covered in oleylamine plus folic acid were further conjugated with oleylamine encapsulated $\text{AgInS}_2\text{-ZnS}$ QDs for HeLa and MCF7 cancer cell staining to show the targeting capability. A quick and straightforward synthesis of strongly NIR-luminescent $\text{AgInSe}_2\text{-ZnSe}$ QDs with tunable emissions in aqueous media was also reported. To make water-soluble $\text{AgInSe}_2\text{-ZnSe}$ QDs, this process avoids high temperatures, pressures, and organic solvents. The $\text{AgInSe}_2\text{-ZnSe}$ QDs' PL peaks could be monitored in the range of 625 to 940 nm, with PL QYs of up to 31% at maximum. As a result, $\text{AgInSe}_2\text{-ZnSe}$ QDs with a high PL QY, NIR emission tunability, and low cytotoxicity can be used for cell labeling and bioimaging²⁵².

2.6 IV-VI Group

Because of their unique electronic and transport properties, group IV-VI SC QDs is an outstanding candidate for biomedical applications²⁵³. Mainly, monodisperse PbS and PbSe QDs are the unique structures in this category. . They have diameters ranging from

3 to 8 nanometers and in the case of PbSe, its lowest-energy exciton transitions occur at wavelengths between 1.0 and 1.85 μm ²⁵⁴. It also has a tunable emission spectrum ranging from 1200 to 1500 nm. PbS/CdS/ZnS, Luc8-PbS complex, PbSe/CdSe core/shell QDs, and GST-EGFP-GB1 protein-coated PbS QDs are some of the other structures that have been created up to now. Due to the low extinction coefficient of tissues in this spectral range, high-quality, water-dispersible QDs probe lying inside the NIR-II window (1000–1350 nm) contributes to higher penetration depths²⁵⁵.

		IIA	IVA	VA	VIA	VIIA
		⁵ B	⁶ C	⁷ N	⁸ O	⁹ F
IB	IIB	¹³ Al	¹⁴ Si	¹⁵ P	¹⁶ S	¹⁷ Cl
²⁹ Cu	³⁰ Zn	³¹ Ga	³² Ge	³³ As	³⁴ Se	³⁵ Br
⁴⁷ Ag	⁴⁸ Cd	⁴⁹ In	⁵⁰ Sn	⁵¹ Sb	⁵² Te	⁵³ I
⁷⁹ Au	⁸⁰ Hg	⁸¹ Tl	⁸² Pb	⁸³ Bi	⁸⁴ Po	⁸⁵ At

Figure 11. Semiconductors from either elements or combinations of group IV and group VI (called IV-VI semiconductors).

Application

Fluorescence Imaging: To obtain the NIR-far red dual emission fluorescence, in Zhao et al.,²⁵⁶ nanohybrid Au nanoclusters (NCs) -PbS-QDs were synthesized using the co-temple process. Since its emission lies in the ‘optical window’ of *in vivo* imaging with significant Stokes shift and brilliant isolation of two emissions, this substance is ideal for high-resolution bio-imaging. PbS QDs and their use for *in vivo* NIR fluorescence imaging of cerebral venous thrombosis in septic mice were stated by Imamura et al.²⁵⁷ Zamberlan et al.²⁵⁸ specified the synthesis of QDs that combine the biocompatibility and stability of DHLA-PEG-ligands with the tunability of PbS QD emission in the NIR range of low biological tissue absorption.

2.8 Layered Semiconductors

2.8.1 Phosphorous (P)

Phosphorus, which belongs to group V of the periodic table, is abundant in nature (0.1 percent of the Earth’s crust)²⁵⁹ and has four allotropes based on its atomic structure⁹⁰.

Black Phosphorous (BP)

BP is a p-type semiconducting^{139,260,261} allotrope of phosphorus, and it has yet to be developed. It was the first single-element layered material to have semiconducting properties outside of group IV, including graphene, silicene, etc²⁶². Phosphorene is the name assigned to a black phosphorus monolayer, where phosphorus atoms are covalently bonded. The term is habitually used to describe numerous stacked monolayers, alternatively known as ‘few-layer phosphorene’ or few-layer BP (FLBP). Those chemical bonds connect the phosphorus atoms in BP to three surrounding phosphorus atoms, and different layers of BP are connected by van der Waals forces^{263,264}.

Additionally, BP has shown to be the most thermodynamically stable allotrope of P element compared to white and red phosphorus. Phosphorene possesses an intrinsic, direct, and significant band gap²⁶⁵, unlike graphene. Among BP current synthesis methods are top-down simple methods that do not require complicated equipment such as mechanical cleavage^{126,266,267}, liquid-phase^{208,268}, and pulsed laser exfoliation^{82,269–271} the latter being the most time-consuming and costly. As mentioned earlier and further, ultrathin, thin-layer BP nanosheets, nanodots, and BP quantum dots can be obtained throughout the processes. Even though chemical vapor deposition (CVD) from wet chemistry^{115,264,272} (bottom-up methods) is a large-scale preparation of graphene and TMDCs, the production of BP by CVD method is relatively rare due to BP surface strong chemical activity. To date, high-energy mechanical milling (HEMM) is a scalable process for creating the right conditions for the production of BP²⁷¹. A comparison of synthetic conditions for preparing BPQDs with different precursors, solvents, and reactions is summarized in Table 5. Most of the processes used the same NMP solvent.

2.1.2.1 Application

Black Phosphorus, specifically nano-sized BP, has specific optical and electronic properties that enable it to be used as a perfect analog to the current materials used in biomedical imaging applications^{265,273–276}. These properties include an accurate optical response, anisotropic charge transport, semiconducting with a layer-dependent bandgap, moderate carrier mobility, sizeable surface-area-to-volume ratio, photoacoustic properties, and excellent biocompatibility and low cytotoxicity, coupled with spontaneous biodegradability. Explorations for basic optical properties of BP have recently been comprehensive, including layer-dependent optical absorption, fluorescent engineering, and polarized Raman behaviors, thanks to its thickness-dependent band structure and anisotropic function²⁷⁷. Furthermore, several surface coating ligands can

customize the BP, allowing it to be used as novel biomaterials. Compared to the other 2D materials and materials above and below mentioned, BP exhibits a layer-dependent bandgap modulated from 0.3 to 2.0 eV corresponding to bulk and single-layer structures, respectively^{111,260,278}. The single layer of free-standing phosphorene has a direct bandgap of 1.0 eV¹³⁹. Therefore, it results in strong absorption in the ultraviolet and NIR regions. Besides, due to the confinement effect, the bandgap of BP is extended to 1.45 eV approximately, resulting in photoluminescence emission at 855 nm⁷³. Notably, in biomedicine, its applications are photothermal therapy, photodynamic therapy (PDT), and, as mentioned: bioimaging.

Photoacoustic imaging: ultrathin BP can be used for internal photoacoustic imaging of tumors due to its photothermal properties and photoacoustic signals^{279,280}. In exposition to water, and air, particularly when humidity²⁸¹, oxygen, and light are simultaneously existing²⁷¹ BP is fast degraded. Then it affects the optical properties and further biological applications. To avoid BP limitation and to better withstand for showing an excellent photoacoustic imaging signal, researchers did enhance solubility, biocompatibility by PEGylation⁹⁰, covalent aryl diazonium functionalization²⁸² Sun et al.⁸⁷ mixed BPQDs with a titanium sulfonate ligand (TiL4; L: titanium *p*-toluene sulfonate), which was previously synthesized in ethanol by reacting titanium tetraisopropoxide [Ti(OiPr)₄] with *p*-toluenesulfonic acid; in N-methyl-2-pyrrolidone to obtain prepared TiL4@BPQDs. These black phosphorus quantum dots coordinated with a sulfonic ester of the titanium ligand exhibit enhanced stability under those exposed-environmental conditions.

Fluorescence Imaging: Besides, since BP nanodots have a layer-dependent fluorescence spectrum, they can emit multiple colors such as blue and green photoluminescence²⁷⁴. Additionally, BP has a large specific surface area; therefore, it can be filled with fluorescent molecules for fluorescence imaging *in vitro* and *in vivo*. On the one hand, for *in vivo* NIR imaging, Tao et al.²⁷⁸ loaded cyanine seven onto PEGylated BP nanosheets and fluorescein isothiocyanate (FITC) onto PEGylated BP nanosheets for *in vitro* fluorescence imaging. On the other hand, Yang et al.²⁸³ used chlorin e6 immobilized-PEGylated BP nanosheets for NIR fluorescence imaging in living animals owing to its outstanding NIR light absorption.

Photothermal Imaging: BP can be used for photothermal imaging using infrared thermography due to its high extinction coefficient and excellent photothermal conversion efficiency. Both prepared biodegradable BPQDs/PLGA nanoparticles and

fabricated PEGylated BP nanoparticles by a modified mechanical milling technique^{90,284} were published in 2016 to improve the photothermal stability of BP. The tumor temperature of mice injected with the BPQDs/PLGA nanospheres increased more quickly than that of mice injected with PBS. Furthermore, the PA signal intensity in the tumor was higher, representing a long retention time.

Surface-Enhanced Raman Scattering Imaging (SERS): is an effective trace analysis technique for detecting analytes at low concentrations and highly sensitive. Its analysis requires prepared BP nanosheets modified with Au nanoparticles (BP–Au NSs). The Au nanostructure improves this BP–Au NSs; thus, it serves as a suitable SERS substrate for Raman biological detection. The photothermal treatment (PTT) impact of BP–Au NSs can be controlled using Raman technology due to the high SERS behavior of BP–Au NSs²⁸⁰. As a result, SERS analysis is used to monitor the PPT effect of the BP–Au NS-based *in vivo*. Hu et al.²⁷⁷ built a BP heterojunction by combining a three-atomic-layer BPQD with a single zinc oxide nanorod (ZnO NR). Due to the adjustment of the heterojunction's surface charge transfer, selective Raman scattering between ZnO and BP could be enhanced by modulating the indium (In) content in ZnO NRs. When the BP concentration is below the parts-per-million level (ppm), the maximum enhancement factor of BP is 4340-fold, and Raman improvement of ZnO can be increased by two orders of magnitude when BPQD is assembled on a single ZnO NRs. Furthermore, BPQD's stability could be improved.

Table 5. Updated methods of BP synthesis for bioimaging. A comparison of synthetic conditions for preparing BP nanostructures with different precursors, solvents, reactions, and methods.

Morphology	Synthesis/ Obtainment Method	Precursors/ Initiators	Conjugated/ Anchored Chemical/Ligand/ Solvent Functionalization	Advantage/ Improvement	Specific imaging technique	Reference/ Year
Few-layer BP (FLBP) Nanosheets	Liquid phase exfoliation Pulsed laser exfoliation High energy mechanical milling (HEMM)	Red phosphorus (RP)-black phosphorus (BP) powders and bulk BP crystals	Stainless steel balls N-methyl-2- pyrrolidone (NMP) solvent.	Highly stable BP in ambient environments. Different sizes and thicknesses can be obtained. Simple, low-cost, tunable process for large-scale applications.	Photothermal Imaging	[271] 2019
	Micromechani cal exfoliation		Same NMP solvent	Increased stability		[281,285] 2017 2018
Thin film	Chemical vapor deposition (CVD)		None	In situ process, successful preparation method. Relative rare		[264] 2016-2018
Ultras small nanosheets (BPQDs)	Liquid exfoliation Ultrasonic exfoliation	Titanium tetrakisopropoxi de [Ti(OiPr) ₄] Bare BPQDs	Titanium sulfonate ligand (TiL ₄) in NMP <i>p</i> -toluene sulfonic acid/ ethanol	Photothermal performance. Stability improved TiL ₄ @BPQDs in aqueous dispersions.	PA	[87,88] 2017 [220] 2016
BPQDs	HEMM	RP	Polyethylene Glycol (PEG)	Water-soluble. Excellent photostability, solventless one-pot process,		PA

			Stainless steel balls.	long retention time and EPR effect.	Photothermal Imaging	[266,280] 2017
Ultrathin BP nanosheets	Liquid exfoliation	BPNSs	Fe ₃ O ₄ NPs Au NPs Deionized water	Low-cost approach for large BP nanocomposite scale production. Broad light absorption band, especially strong NIR absorbance.	MRI guided	[35] 2017
BP nanosheets (BPNSs)	Modified mechanical exfoliation	Bulk BP	Loaded cyanine 7-PEG-amine. (PEG-NH ₂) Oxygen molecule-free water solvent.	Improved biocompatibility and remarkable physiological stability in PBS and cell culture medium. For <i>in vivo</i> NIR imaging. No organic solvent-associated toxicity. Clean BP surface for medical use.	Fluorescence Imaging	[278] 2017
	Liquid exfoliation	Bulk BP	Chlorine e6 (Ce6)-decorated PEG-NH ₂ BPNSs	Good biocompatibility. <i>In vivo</i> FI agent. Outstanding NIR light absorption due to Ce6.	Fluorescence Imaging Thermal Imaging	[283] 2018
		Bulk BP crystals	NMP Chloroauric acid (HAuCl ₄ ·4H ₂ O)	Improved absorption in NIR region, excellent photostability, outstanding photothermal transfer efficiency. Au NPs enhance efficiency for an effective substrate.	Surface-Enhanced Raman Scattering Imaging (SERS) SERS	[286] 2017
	Solvothermal method	White phosphorus	Isopropyl alcohol (IPA) ZnO NRs Polar NMP solvent Ethylenediamine solvent	Excellent dispersity, ambient stability, improved thermal conductivity. Excellent stability due to partial oxidation of the surface. The scalable, low-cost, one-step process at low temperature. Conceptually simple	Fluorescence Imaging	[277] 2018 [115] 2018

Chapter III

3 Chemical method vs. Green method

Surfactants, material composition, structure, and reaction conditions became as crucial as precursor chemistry as the majority of other binary inorganic semiconducting structures (notably the IV-VIs and III-Vs) were prepared using similar chemistry, progressing from organometallic to inorganic and silylated precursors. Aside from the various synthesis methods mentioned in the preceding section, researchers have attempted to discover and achieve novel production methods for SC assemblies. Besides, in the current literature, two separate basic concepts of synthesis (i.e., top-down and bottom-up methods) have been studied to obtain nanomaterials of ideal sizes, shapes, and functionalities.

NMP and IPA are the most efficient solvents for reducing the energy needed for exfoliation⁴⁸. Depending on the synthesis platform used, QDs may be prepared using physical, chemical, or biological methods. Physical synthesis methods like laser physical vapor deposition²⁸⁷ and laser irradiation of large particles are simple, timesaving, and environmentally friendly²⁸⁸⁻²⁹⁰. Depending on the ultrasound's mechanical effect, exfoliation by ultrasonication in liquids containing different solvents, surfactants, and polymers can create single-layer nanosheets on a large scale. Figure 12 depicts the most used chemical methods, including the green chemical process.

3.1 Green Synthesis (either from plant extracts or from nutrients)

Some QDs with an average thickness of a few nanometers are hard to come by. As a result, developing a green strategy for fabricating them is critical and remains a difficult task. A new wave of 'green synthesis' approaches/methods is gaining traction in contemporary materials science, technology research and development to overcome these limits. The green synthesis with the ease of high-quality colloidal QDs is critical and highly awaited. However, it has not yet been completely realized. Green synthesis of

materials/ nanomaterials, which is achieved by supervision, monitoring, cleanup, and remediation, would help improve their environmental friendliness. In terms of green synthesis, synthetic synthesis methods, chemical vapor deposition, and mechanical exfoliation are very similar. This is because none of the before mentioned systems use toxic chemicals. The solvents NMP and IPA are used in many applications. Biologically, the levels of NMP metabolites excreted in the urine following contact were about > 65% of the administered doses, respectively. In rabbits, NMP has a low risk of skin irritation and a high risk of eye irritation. Compared to ethanol, IPA evaporates quickly, leaving virtually no oil residue, and is comparatively non-toxic compared to alternative solvents. As a result, they are not a threat. Several elements, such as waste prevention/minimization, derivatives/pollution control, and the use of safer (or non-toxic) solvents/auxiliaries, as well as sustainable feedstock, can thus be demonstrated by certain fundamental concepts of "green synthesis." Green syntheses are necessary to prevent unnecessary or unhealthy by-products by developing reliable, sustainable, and environmentally friendly syntheses. To achieve this purpose, ideal solvent systems and natural resources (such as organic systems) are needed. To fit different biological materials, green synthesis of metallic nanoparticles has been used (e.g., bacteria, fungi, algae, and plant extracts).

3.1.1 Some green synthesis advances in SC QDs

Biosynthesis of nanoparticles is critical in developing sustainable technology, especially for the environment, because of its cost-effectiveness and environmental friendliness, providing a viable alternative to chemical and physical methods. Green synthesis connects nanotechnology and biotechnology to synthesize biocompatible, stable NPs, based on the twelve principles of Green chemistry¹³⁸. Plant extracts, microorganisms, and viruses or their extracts are used as biological routes for large-scale NP processing due to their antioxidant and reducing properties. Biosynthetic processes, on the other hand, not only work under moderate conditions yet also have higher biocompatibility and biostability since their development (by the attachment of biomolecules to their structure) occurs without the need for additional stages of functionalization and encapsulation^{142,291,292}, providing a green synthesis route for preparing biocompatible QDs. Biosynthesized QDs, including chemically synthesized QDs, have customizable spectral emission windows and simultaneous excitation of QDs of various sizes using a single light source.

It has recently become more popular to synthesize monodisperse QDs under milder reaction conditions. To manufacture CdTe QDs with quantum yields as high as 75% before passivation, these methods use lower temperatures (100°C), green chemicals like cadmium acetate ($\text{Cd}(\text{Ac})_2$), and a thiolated capping agent in aqueous solution²⁹³.

Deng et al. used dihydrolipoic acid (DHLA) as a stabilizer to create a simple and environmentally safe water-soluble PbS QD with heavy fluorescence in the NIR spectral range 870–1010 nm²⁹⁴. In contrast, while size-tunable PbS synthesis between 3 and 10 nm with NIR II emission is well-known, there is no well-established method for producing smaller particles with emission below 1000 nm, which are easier to detect with less expensive and more commonly available Si and extended PMT-detectors. At low temperatures (65–80 °C), Durmusoglu et al.²⁹⁵ demonstrated the synthesis of PbS QDs varying in scale from 2.4 to 3.2 nanometers using PbCl_2 , elemental sulphur, dodecanethiol (DT), and a toluene/oleylamine mixture. It was discovered that adding DT increases the solubility of sulphur and that DT binds to the crystal surface during development, resulting in a smaller crystal with higher luminescence strength. The addition of toluene as a cosolvent lowers the viscosity while still reducing the bulk. Size-tunable synthesis of strongly luminescent QDs was achieved using these variables.

Furthermore, as a post-process, there was the use of additional DT ligand exchange to improve long-term particle stability. The luminescence properties of OLA/DT and DT-capped PbS QDs were investigated using photoluminescence lifetimes. Finally, a successfully extend synthesis process to produce tiny PbSe QDs was achieved.

In Caires' et al.²⁹⁶ work, ZnS fluorescent quantum dots (ZnS-QDs) were synthesized and stabilized as a pH-sensitive biopolymer by carboxymethylcellulose (CMC) using a simple one-step green aqueous colloidal procedure at different pH conditions (acidic, neutral, and alkaline) and chemical proportions of precursors (Zn^{2+} , S^{2-}). UV–visible and photoluminescence spectroscopy is used to describe these nanoconjugates' optical properties (ZnS@CMC).

CuInS_2 QDs with tunable emission from visible to NIR range (max emission covers 675–835 nm) were recorded by Qi et al.²⁹⁷, with PL QYs of up to 8.7% observed by simply regulating the reaction time. NIR emitting CDs (R-CDs) were successfully prepared by Li et al. using spinach as a precursor. It allows the bio-tissues suffer from less autofluorescence and less harm from absorption radiation. The R-CDs had good water

solubility, excellent photo-stability, an emission peak at 680 nm, a PL QY of 15.34 %, good compatibility, and low toxicity. With lung cancer cells (A549) excited at 543 nm, R-CDs was an excellent cellular labeling agent²⁹⁸.

In Oliveira et al.²⁹⁹ is reported the syntheses of Luminescent CdTe Quantum Dots on a Long-Term Basis. CdTeQDs@MNs, a family of stable luminescent nanoparticles consisting of quantum dots coated with modified mesoporous silica nanoparticles, have been synthesized and fully characterized. The involvement of luminescent QDs enables imaging of nanoparticles during cell internalization and visualization of doxorubicin selective release within the cell (via pH stimuli).

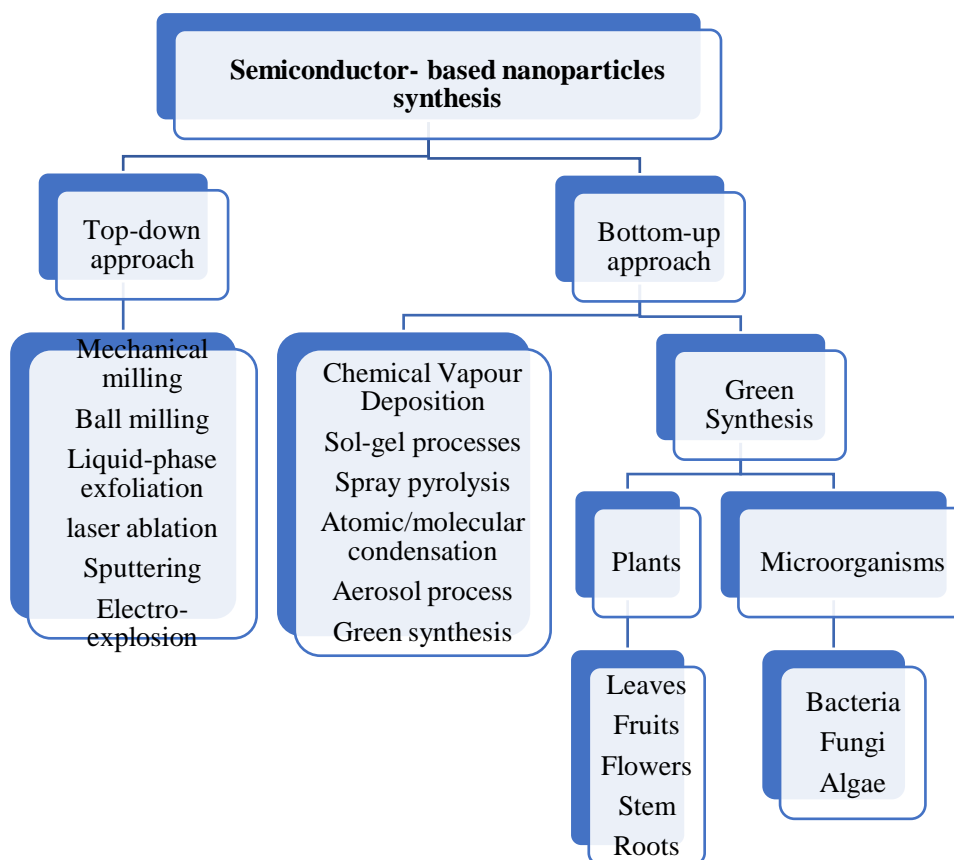


Figure 12. Synthesis classification for nanoparticles as a whole

Extremely photoluminescent Ag₂Se quantum dots (QDs) with emission at 1300 nm in the second near-infrared window have been synthesized by Dong et al.³² using a simple solvothermal process. The Ag₂Se QDs have bright photoluminescence, good water solubility, high colloidal stability and photostability, and good biocompatibility after surface modification of C18-PMH-PEG. They are also successfully used *in vivo* deep imaging of organs and vascular systems with high spatial resolution. With its tiny footprint, perfect optical properties, and good biocompatibility, this recent NIR-II

fluorescent nanoprobe opens up exciting possibilities for potential biomedical applications. However, Armijo et al.³⁰⁰ synthesized Silver Selenide (Ag_2Se) nanostructures by combining silver nitrate (AgNO_3) and selenous acid (H_2SeO_3) as Ag and Se sources respectively while; fructose and starch act as reducing and stabilizing agents, respectively. The sonochemistry-mediated procedure was carried out with water as the solvent at low temperature, following Green Chemistry standards. Their cellular essays confirm the low cytotoxicity. Therefore, it promises a new more biocompatible green material for bioimaging.

In Bharathi et al.³⁰¹, research focuses on the cellular absorption of nanomaterials in biomedical applications. Using a green strategy, we developed a water-soluble lead sulfide quantum dot (PbS QD) with glutathione as the stabilizing ligand and 3-MPA (mercaptopyropionic acid) as the stabilizing ligand. Because of its high conjugation efficiency, 3-MPA-capped QDs were further modified with streptavidin and then bound to biotin. These bio-conjugated QDs were tested for cell labeling and bio-imaging. These materials are ideal for deep tissue imaging due to the bright red fluorescence of these types of QDs in HeLa cells.

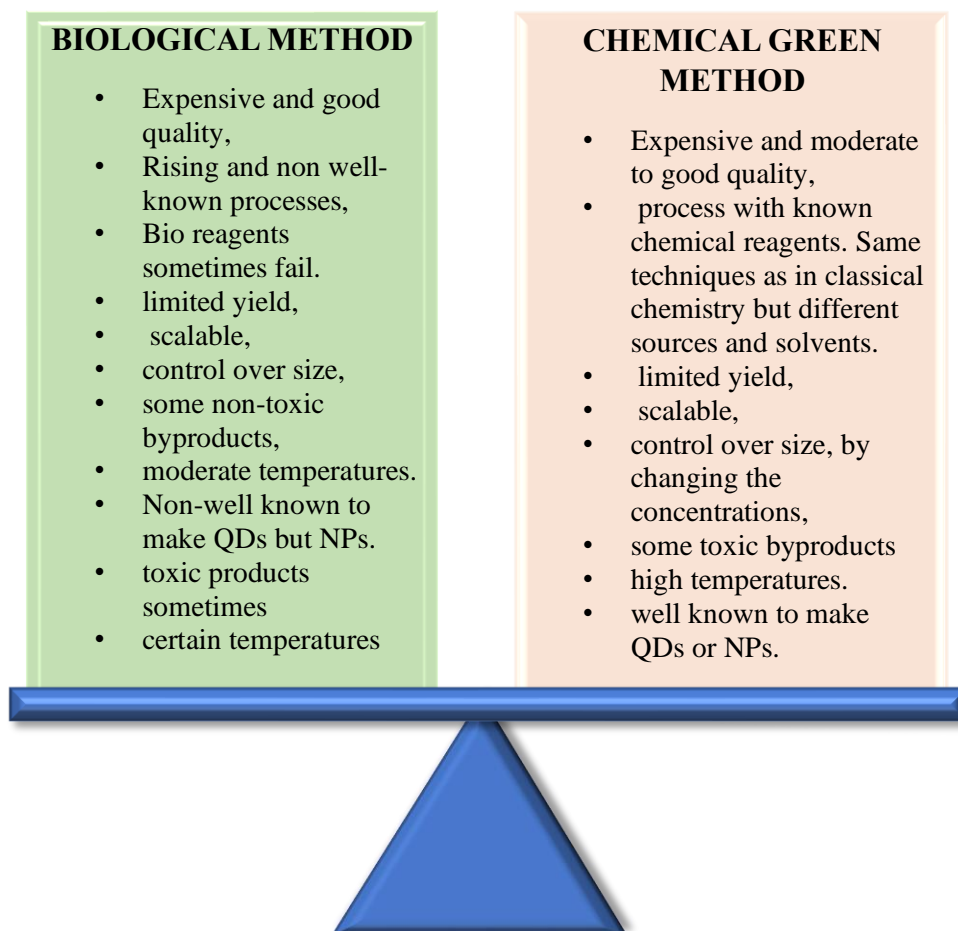


Figure 13. Green synthesis vs. Different synthetic methods. Main characteristics

Chapter IV

Conclusion and Outlook

While research into semiconductor-based nanoparticles' biomedical applications has progressed significantly, there are still some issues to be resolved before clinical application. On the one hand, since some different sized-QDs have such a significant impact on toxicity and treatment results, it is critical to developing a novel method for fabricating them with uniform size and high production. Second, other therapies, such as chemotherapy and immunotherapy, may be used in combination with several nanomaterials to achieve a synergistic impact. Parenthetically, it is preferable to combine MRI, CT, and PA organically to obtain detailed diagnostic and overcome the inherent limitations of single-mode imaging. As a result, new flexible nanoplatfoms for combined multimodal imaging are still required to achieve a definitive diagnosis. The newly non-invasive optical therapy, which includes photothermal therapy (PTT) and photodynamic therapy (PDT), could be combined and guided by MRI/CT/PA multimodalities. Following nearly a decade of intense effort in developing semiconductor quantum dots' growth, synthesis, material selection, and characterization, progress in the last few years has been characterized in terms of the types of applications for which these structures are most suitable. In this short work, the compilation of a selection of recent quantum dot developments for one of the biomedical applications highlights state of the art: imaging was attempted. For the year 2020, a simple literature search on the phrase "semiconductor quantum dots imaging" yields more than 5.900 citations. Clearly, in this literature analysis, we were just able to scratch the surface. Thus, this requires multidisciplinary researchers to work together to exploit the great potential in biomedicine. Fig. 13 summarizes and compares conventional biological and chemical approaches; green NP synthesis has many benefits. There is no requirement for high-pressure machines in addition to operating at moderate temperatures. Furthermore, the risk of disposing of solvents and toxic waste is significantly minimized. Overall, going green is easy and cost-effective because it uses recycled natural materials and produces more sustainable and safe goods³⁰². Regarding to layered semiconductors, to date, there are few published

essays, articles, papers on either novel synthesis or green enhancement processes. Also, many other researchers have achieved outstanding photothermal imaging by different modifications of these structures.

Annexes

Table 6. Overall classification of semiconductors according to their group, alloys, and structure.

IV Group	Elemental Semiconductors		Compound Semiconductors	
	Carbon (C) Silicon (Si)	Germanium (Ge)	Silicon Phosphide (SiP)	
III-V Group	Alloys			
	Simple		Triple	
	Boron:		Aluminum:	
	Boron nitride (BN)		Aluminum antimonide (AlSb)	
	Boron phosphide (BP)		Aluminum arsenide (AlAs)	
	Boron arsenide (BAs)		Aluminum nitride (AlN)	
	Gallium:		Aluminum phosphide (AlP)	
	Gallium antimonide (GaSb)		Gallium Aluminum Arsenide (AlGaAs, Al _x Ga _{1-x} As)	
	Gallium arsenide (GaAs)		Gallium-Indium Arsenide (InGaAs, In _x Ga _{1-x} As)	
	Gallium nitride (GaN)		Indium Gallium Phosphide (InGaP)	
Gallium phosphide (GaP)		Indium Aluminum Arsenide (AlInAs)		
Indian:		Indium aluminum antimonide (AlInSb)		
Indium antimonide (InSb)		Gallium-arsenic nitride (GaAsN)		
Indium arsenide (InAs)		Gallium arsenic phosphide (GaAsP)		
Indium nitride (InN)		Gallium Aluminum Nitride (AlGaN)		
Indium phosphide (InP)		Gallium Aluminum Phosphide (AlGaP)		
		Gallium-Indium Nitride (InGaN)		
		Indium-arsenic antimonide (InAsSb)		
		Gallium-indium antimonide (InGaSb)		
		Quadruple		
		Quintuple		
		Gallium-indium-nitrogen-arsenic antimonide (GaInNASb)		
		Triple Alloys		
		Cadmium-zinc telluride (CdZnTe)		
		Mercury-cadmium telluride (HgCdTe)		
		Mercury-zinc telluride (HgZnTe)		
		Mercury-zinc selenium (HgZnSe)		
II-VI Group	Cadmium selenide (CdSe)	Zinc selenide (ZnSe)		
	Cadmium sulfide (CdS)	Zinc sulfide (ZnS)		
	Cadmium telluride (CdTe)	Zinc telluride (ZnTe)		
	Zinc oxide (ZnO)			
V-VI Group	Bismuth telluride (Bi ₂ Te ₃)			
I-VI Group	Copper sulfide CuS			
I-VII Group	Copper Chloride (CuCl)			
IV-VI Group	Lead selenide (PbSe)	Tin sulfide (SnS)	Triple alloys	
	Lead Sulfide (PbS)	Tin telluride (SnTe)		
	Lead telluride (PbTe)			
II-V Group	Cadmium phosphide (Cd ₃ P ₂)	Zinc phosphide (Zn ₃ P ₂)		
	Cadmium arsenide (Cd ₃ As ₂)	Zinc arsenide (Zn ₃ As ₂)		
	Cadmium antimonide (Cd ₃ Sb ₂)	Zinc antimonide (Zn ₃ Sb ₂)		
			Lead-tin telluride (PbSnTe)	
			Thallium-lead telluride (Tl ₂ SnTe ₅)	
			Thallium-germanium telluride (Tl ₂ GeTe ₅)	

Layered SC	Tin (II) iodide (SnI ₂)	Bismuth sulfide (Bi ₂ S ₃)	Bismuth Iodide II (BiI ₃)
	Molybdenum disulfide (MoS ₂)	Copper Indium Gallium Selenide (CIGS)	Mercury Iodide II (HgI ₂)
	Gallium selenide (GaSe)	Platinum Silicide (PtSi)	Thallium bromide (TlBr)
	Tin sulfide (SnS)		
Oxides SC	Oxides	Dioxides	Trioxides
	Copper (I) oxide (Cu ₂ O)	Titanium dioxide (TiO ₂)	Uranium trioxide (UO ₃)
	Copper (II) oxide (CuO)	Uranium dioxide (UO ₂)	
Organic	Polymer Semiconductor		
Magnetic	GaMnAs		

References

1. Christian Röthig GS. *CFN Lectures on Functional Nanostructures - Volume 2: Nanoelectronics - Google Libros*. Springer ; 2011. Accessed May 16, 2021. https://books.google.com.mx/books?id=NvgaswEACAAJ&dq=nanostructures&hl=es-419&sa=X&ved=2ahUKEwicsYLw68_wAhURKK0KHcF0Av0Q6AEwAXoECAMQAg
2. Cao G, Wang Y. *Nanostructures and Nanomaterials*. Vol 2. WORLD SCIENTIFIC; 2011. doi:10.1142/7885
3. Pájaro Castro N, Olivero Verbel J, Redondo Padilla J. Nanotecnología aplicada a la medicina. *Rev Guillermo Ockham*. 2013;11(1):125. doi:10.21500/22563202.606
4. semiconductor | Definition, Examples, Types, Uses, Materials, Devices, & Facts | Britannica. Accessed April 15, 2021. <https://www.britannica.com/science/semiconductor>
5. Gunn G. *Critical Metals Handbook*.; 2014. Accessed May 17, 2021. www.wiley.com/wiley-blackwell.
6. Prokof'ev VY, Naumov VB, Dorofeeva VA. Gallium concentration in natural melts and fluids. *Geochemistry Int*. 2016;54(8):691-705. doi:10.1134/S0016702916080097
7. Gunkel G, Beulker C, Grupe B, Gernet U, Viteri F. Aluminium in Lake Cuicocha, Ecuador, an Andean Crater Lake: Filterable, Gelatinous and Microcrystal Al Occurrence. *Aquat Geochemistry*. 2011;17(2):109-127. doi:10.1007/s10498-010-9114-z
8. Peñafiel-Vicuña S, Rendón-Enríquez I, Vega-Poot A, López-Téllez G, Palma-Cando A, Frontana-Urbe BA. Recovering Indium Tin Oxide Electrodes for the Fabrication of Hematite Photoelectrodes. *J Electrochem Soc*. 2020;167(12):126512. doi:10.1149/1945-7111/abaf7a
9. Dalgo D, Ochoa-Herrera V, Parra R, Peñafiel R. MONOIL Monitoring of Oil activities in Ecuador: a cross-disciplinary approach between Environment, Health and People View project Air quality in Ecuador View project. doi:10.18272/aci.v7i2.272
10. De La Torre E, Vargas E, Ron C, Gámez S. Europium, yttrium, and indium recovery from electronic wastes. *Metals (Basel)*. 2018;8(10):777. doi:10.3390/met8100777
11. de Koning GHJ, Veldkamp E, López-Ulloa M. Quantification of carbon sequestration in soils following pasture to forest conversion in northwestern Ecuador. *Global Biogeochem Cycles*. 2003;17(4):1098. doi:10.1029/2003gb002099
12. Atiaga O, Nunes LM, Otero XL. Effect of cooking on arsenic concentration in

- rice. *Environ Sci Pollut Res.* 2020;27(10):10757-10765. doi:10.1007/s11356-019-07552-2
13. Otero XL, Tierra W, Atiaga O, et al. Arsenic in rice agrosystems (water, soil and rice plants) in Guayas and Los Ríos provinces, Ecuador. *Sci Total Environ.* 2016;573:778-787. doi:10.1016/j.scitotenv.2016.08.162
 14. Atiaga-Franco OL, Otero XL, Gallego-Picó A, Escobar-Castañeda LA, Bravo-Yagüe JC, Carrera-Villacrés D. Analysis of total arsenic content in purchased rice from Ecuador. *Czech J Food Sci.* 2019;37(6):425-431. doi:10.17221/183/2018-CJFS
 15. Cumbal L, Vallejo P, Rodriguez B, Lopez D. Arsenic in geothermal sources at the north-central Andean region of Ecuador: Concentrations and mechanisms of mobility. *Environ Earth Sci.* 2010;61(2):299-310. doi:10.1007/s12665-009-0343-7
 16. *The Origin of Arsenic in Waters and Sediments from Papallacta Lake Area in Ecuador - USQ EPrints.* Accessed May 17, 2021. <https://eprints.usq.edu.au/26263/>
 17. Hamer U, Potthast K, Burneo JI, Makeschin F. Nutrient stocks and phosphorus fractions in mountain soils of Southern Ecuador after conversion of forest to pasture. *Biogeochemistry.* 2013;112(1-3):495-510. doi:10.1007/s10533-012-9742-z
 18. Goller R, Wilcke W, Fleischbein K, Valarezo C, Zech W. Dissolved nitrogen, phosphorus, and sulfur forms in the ecosystem fluxes of a montane forest in Ecuador. *Biogeochemistry.* 2006;77(1):57-89. doi:10.1007/s10533-005-1061-1
 19. Leary S, Sillitoe RH, Stewart PW, Roa KJ, Nicolson BE. Discovery, geology, and origin of the Fruta del Norte epithermal gold-silver deposit, southeastern Ecuador. *Econ Geol.* 2016;111(5):1043-1072. doi:10.2113/econgeo.111.5.1043
 20. *Cadmium Distribution in Ecuadorian Cacao Beans during Post-Harvest Processes.*
 21. (15) (PDF) Energy Band Theory & Classification of Solids. Accessed April 15, 2021. https://www.researchgate.net/publication/286862888_Energy_Band_Theory_Classification_of_Solids/figures?lo=1
 22. Tupei Chen YL. *Semiconductor Nanocrystals and Metal Nanoparticles: Physical Properties and ...* - Google Libros. Accessed April 15, 2021. https://books.google.com.ec/books?hl=es&lr=&id=rhQNDgAAQBAJ&oi=fnd&pg=PP1&dq=Semiconductor+V-VI+Quantum+Dots+and+Their+Biomedical+Applications+&ots=wPT5RDzPsB&sig=u_Pt025ydF_4akVTklSbEV_8miY#v=onepage&q&f=false
 23. Pallab Bhattacharya, Roberto Fornari, Hiroshi Kamimura. *Comprehensive Semiconductor Science and Technology* - Google Libros. Accessed April 15, 2021. <https://books.google.com.ec/books?hl=es&lr=&id=PYxBKNI8tw8C&oi=fnd&pg=PP2&dq=Semiconductor+V-VI+Quantum+Dots+and+Their+Biomedical+Applications+&ots=VzbH0B8Ixx&>

sig=vR75ZwMjRWYp4DCydDDUS8GvZKk#v=onepage&q&f=false

24. Pantelides ST. The electronic structure of impurities and other point defects in semiconductors. *Rev Mod Phys.* 1978;50(4):797-858. doi:10.1103/RevModPhys.50.797
25. Busch P, Heinonen T, Lahti P. Heisenberg's uncertainty principle. *Phys Rep.* 2007;452(6):155-176. doi:10.1016/j.physrep.2007.05.006
26. Sellin PJ. Thick film compound semiconductors for X-ray imaging applications. *Nucl Instruments Methods Phys Res Sect A Accel Spectrometers, Detect Assoc Equip.* 2006;563(1):1-8. doi:10.1016/j.nima.2006.01.110
27. Owens A. Semiconductor materials and radiation detection. *J Synchrotron Radiat.* 2006;13(2):143-150. doi:10.1107/S0909049505033339
28. Kyle S, Saha S. Nanotechnology for the Detection and Therapy of Stroke. *Adv Healthc Mater.* 2014;3(11):1703-1720. doi:10.1002/adhm.201400009
29. Zhou Z, Kong B, Yu C, et al. Tungsten oxide nanorods: An efficient nanoplatform for tumor CT imaging and photothermal therapy. *Sci Rep.* 2014;4. doi:10.1038/srep03653
30. Reineck P, Gibson BC. Near-Infrared Fluorescent Nanomaterials for Bioimaging and Sensing. *Adv Opt Mater.* 2017;5(2). doi:10.1002/adom.201600446
31. Ren L, Liu X, Ji T, et al. "all-in-One" Theranostic Agent with Seven Functions Based on Bi-Doped Metal Chalcogenide Nanoflowers. *ACS Appl Mater Interfaces.* 2019;11(49):45467-45478. doi:10.1021/acscami.9b16962
32. Dong B, Li C, Chen G, et al. Facile synthesis of highly photoluminescent Ag₂Se quantum dots as a new fluorescent probe in the second near-infrared window for in vivo imaging. *Chem Mater.* 2013;25(12):2503-2509. doi:10.1021/cm400812v
33. Granada-Ramírez DA, Arias-Cerón JS, Rodríguez-Fragoso P, et al. *Quantum Dots for Biomedical Applications.* Elsevier Ltd.; 2018. doi:10.1016/B978-0-08-100716-7.00016-7
34. Erogbogbo F, Chang CW, May JL, et al. Bioconjugation of luminescent silicon quantum dots to gadolinium ions for bioimaging applications. *Nanoscale.* 2012;4(17):5483-5489. doi:10.1039/c2nr31002c
35. Yang D, Yang G, Yang P, et al. Assembly of Au Plasmonic Photothermal Agent and Iron Oxide Nanoparticles on Ultrathin Black Phosphorus for Targeted Photothermal and Photodynamic Cancer Therapy. *Adv Funct Mater.* 2017;27(18). doi:10.1002/adfm.201700371
36. Jing L, Ding K, Kershaw S V., Kempson IM, Rogach AL, Gao M. Magnetically Engineered Semiconductor Quantum Dots as Multimodal Imaging Probes. *Adv Mater.* 2014;26(37):6367-6386. doi:10.1002/adma.201402296
37. Dallas J, Pavlidis G, Chatterjee B, et al. Thermal characterization of gallium nitride p-i-n diodes. *Appl Phys Lett.* 2018;112(7). doi:10.1063/1.5006796
38. Yang X, Wang D, Shi Y, Zou J, Zhao Q. Black Phosphorus Nanosheets Immobilizing Ce6 for Imaging Guided Photothermal / Photodynamic Cancer Therapy. *ACS Appl Mater Interfaces.* Published online 2018.

doi:10.1021/acsami.8b00276

39. Liu T, Shi S, Liang C, et al. Iron oxide decorated MoS₂ nanosheets with double PEGylation for chelator-free radiolabeling and multimodal imaging guided photothermal therapy. *ACS Nano*. 2015;9(1):950-960. doi:10.1021/nn506757x
40. Rojas S, Gispert JD, Abad S, et al. In vivo biodistribution of amino-functionalized ceria nanoparticles in rats using positron emission tomography. *Mol Pharm*. 2012;9(12):3543-3550. doi:10.1021/mp300382n
41. Zahin N, Anwar R, Tewari D, et al. Nanoparticles and its biomedical applications in health and diseases: special focus on drug delivery. *Environ Sci Pollut Res*. 2020;27(16):19151-19168. doi:10.1007/s11356-019-05211-0
42. Yao J, Li P, Li L, Yang M. Biochemistry and biomedicine of quantum dots: from biodetection to bioimaging, drug discovery, diagnostics, and therapy. *Acta Biomater*. 2018;74:36-55. doi:10.1016/j.actbio.2018.05.004
43. Ma D, Zhao J, Xie J, et al. Ultrathin boron nanosheets as an emerging two-dimensional photoluminescence material for bioimaging. *Nanoscale Horizons*. 2020;5(4):705-713. doi:10.1039/c9nh00698b
44. Li Z, Wong SL. Functionalization of 2D transition metal dichalcogenides for biomedical applications. *Mater Sci Eng C*. 2017;70:1095-1106. doi:10.1016/j.msec.2016.03.039
45. Qian X, Shen S, Liu T, Cheng L, Liu Z. Two-dimensional TiS₂ nanosheets for in vivo photoacoustic imaging and photothermal cancer therapy. *Nanoscale*. 2015;7(14):6380-6387. doi:10.1039/c5nr00893j
46. Li Z, Wong SL. Functionalization of 2D transition metal dichalcogenides for biomedical applications. *Mater Sci Eng C*. 2017;70:1095-1106. doi:10.1016/j.msec.2016.03.039
47. Zhang H, Wu H, Wang J, et al. Graphene oxide-BaGdF₅ nanocomposites for multi-modal imaging and photothermal therapy. *Biomaterials*. 2015;42:66-77. doi:10.1016/j.biomaterials.2014.11.055
48. Chen Y, Tan C, Zhang H, Wang L. Two-dimensional graphene analogues for biomedical applications. *Chem Soc Rev*. 2015;44(9):2681-2701. doi:10.1039/c4cs00300d
49. Zhu S, Zhang J, Qiao C, et al. Strongly green-photoluminescent graphene quantum dots for bioimaging applications. *Chem Commun*. 2011;47(24):6858-6860. doi:10.1039/c1cc11122a
50. He XP, Tian H. Photoluminescence Architectures for Disease Diagnosis: From Graphene to Thin-Layer Transition Metal Dichalcogenides and Oxides. *Small*. 2016;12(2):144-160. doi:10.1002/smll.201502516
51. Peng J, Wang S, Zhang PH, Jiang LP, Shi JJ, Zhu JJ. Fabrication of graphene quantum dots and hexagonal boron nitride nanocomposites for fluorescent cell imaging. *J Biomed Nanotechnol*. 2013;9(10):1679-1685. doi:10.1166/jbn.2013.1663
52. Paredes JI, Villar-Rodil S. Biomolecule-assisted exfoliation and dispersion of

- graphene and other two-dimensional materials: A review of recent progress and applications. *Nanoscale*. 2016;8(34):15389-15413. doi:10.1039/c6nr02039a
53. Ulstrup S, Koch RJ, Schwarz D, et al. Imaging microscopic electronic contrasts at the interface of single-layer WS₂ with oxide and boron nitride substrates. *Appl Phys Lett*. 2019;114(15). doi:10.1063/1.5088968
 54. Abu Saleh D, Sosnik A. Enhanced photoluminescence of boron nitride quantum dots by encapsulation within polymeric nanoparticles. *Nanotechnology*. 2021;32(19):195104. doi:10.1088/1361-6528/abe155
 55. Qayyum MS, Hayat H, Matharu RK, Tabish TA, Edirisinghe M. Boron nitride nanoscrolls: Structure, synthesis, and applications. *Appl Phys Rev*. 2019;6(2). doi:10.1063/1.5092547
 56. Chen X, Boulos RA, Dobson JF, Raston CL. Shear induced formation of carbon and boron nitride nano-scrolls. *Nanoscale*. 2013;5(2):498-502. doi:10.1039/c2nr33071g
 57. Kuthati Y, Kankala RK, Lee CH. Layered double hydroxide nanoparticles for biomedical applications: Current status and recent prospects. *Appl Clay Sci*. 2015;112-113:100-116. doi:10.1016/j.clay.2015.04.018
 58. Mishra G, Dash B, Pandey S. Layered double hydroxides: A brief review from fundamentals to application as evolving biomaterials. *Appl Clay Sci*. 2018;153:172-186. doi:10.1016/j.clay.2017.12.021
 59. Wen J, Yang K, Huang J, Sun S. Recent advances in LDH-based nanosystems for cancer therapy. *Mater Des*. 2021;198:109298. doi:10.1016/j.matdes.2020.109298
 60. Gunawan P, Xu R. Direct assembly of anisotropic layered double hydroxide (LDH) nanocrystals on spherical template for fabrication of drug-LDH hollow nanospheres. *Chem Mater*. 2009;21(5):781-783. doi:10.1021/cm803203x
 61. Kim JH, Park K, Nam HY, Lee S, Kim K, Kwon IC. Polymers for bioimaging. *Prog Polym Sci*. 2007;32(8-9):1031-1053. doi:10.1016/j.progpolymsci.2007.05.016
 62. Kusmieriek E. A CeO₂ semiconductor as a photocatalytic and photoelectrocatalytic material for the remediation of pollutants in industrial wastewater: A review. *Catalysts*. 2020;10(12):1-54. doi:10.3390/catal10121435
 63. Tok AIY, Du SW, Boey FYC, Chong WK. Hydrothermal synthesis and characterization of rare earth doped ceria nanoparticles. *Mater Sci Eng A*. 2007;466(1-2):223-229. doi:10.1016/j.msea.2007.02.083
 64. Li H, Yang ZY, Liu C, et al. PEGylated ceria nanoparticles used for radioprotection on human liver cells under γ -ray irradiation. *Free Radic Biol Med*. 2015;87:26-35. doi:10.1016/j.freeradbiomed.2015.06.010
 65. Yang H, Huang C, Tang A, Zhang X, Yang W. Microwave-assisted synthesis of ceria nanoparticles. *Mater Res Bull*. 2005;40(10):1690-1695. doi:10.1016/j.materresbull.2005.05.014
 66. Habib IY, Kumara NTRN, Lim CM, Mahadi AH. Dynamic light scattering and zeta potential studies of ceria nanoparticles. *Solid State Phenom*. 2018;278

SSP:112-120. doi:10.4028/www.scientific.net/SSP.278.112

67. Kogan MJ, Olmedo I, Hosta L, Guerrero AR, Cruz LJ, Albericio F. Peptides and metallic nanoparticles for biomedical applications. *Nanomedicine*. 2007;2(3):287-306. doi:10.2217/17435889.2.3.287
68. Li RQ, Wang BL, Gao T, et al. Monolithic electrode integrated of ultrathin NiFeP on 3D strutted graphene for bifunctionally efficient overall water splitting. *Nano Energy*. 2019;58:870-876. doi:10.1016/j.nanoen.2019.02.024
69. Huang Z, Liu X, Deng G, et al. One-step assembly of CuMo₂S₃ nanocrystals for the synergistic effect of photothermal therapy and photodynamic therapy. *Dalt Trans*. 2018;47(16):5622-5629. doi:10.1039/c7dt04901c
70. Kasouni A, Chatzimitakos T, Stalikas C. Bioimaging Applications of Carbon Nanodots: A Review. *C*. 2019;5(2):19. doi:10.3390/c5020019
71. Guo W, Dong Z, Xu Y, et al. Sensitive Terahertz Detection and Imaging Driven by the Photothermoelectric Effect in Ultrashort-Channel Black Phosphorus Devices. *Adv Sci*. 2020;7(5). doi:10.1002/advs.201902699
72. Yao K, Yanev E, Chuang HJ, et al. Continuous Wave Sum Frequency Generation and Imaging of Monolayer and Heterobilayer Two-Dimensional Semiconductors. *ACS Nano*. 2020;14(1):708-714. doi:10.1021/acsnano.9b07555
73. Liu H, Neal AT, Zhu Z, et al. Phosphorene: An unexplored 2D semiconductor with a high hole mobility. *ACS Nano*. 2014;8(4):4033-4041. doi:10.1021/nn501226z
74. Robinson J, Xi K, Kumar RV, et al. Size dependent optical properties of MoS₂ nanoparticles and their photo-catalytic applications. *J Phys Energy*. 2020;2:0-31.
75. Xu Y, Yuan J, Fei L, et al. Selenium-Doped Black Phosphorus for High-Responsivity 2D Photodetectors. *Small*. 2016;12(36):5000-5007. doi:10.1002/sml.201600692
76. Jacobs-Gedrim RB, Shanmugam M, Jain N, et al. Extraordinary photoresponse in two-dimensional In₂Se₃ nanosheets. *ACS Nano*. 2014;8(1):514-521. doi:10.1021/nn405037s
77. Wan C, Gu X, Dang F, et al. Flexible n-type thermoelectric materials by organic intercalation of layered transition metal dichalcogenide TiS₂. *Nat Mater*. 2015;14(6):622-627. doi:10.1038/nmat4251
78. Qian X, Shen S, Liu T, Cheng L, Liu Z. Two-dimensional TiS₂ nanosheets for in vivo photoacoustic imaging and photothermal cancer therapy. *Nanoscale*. 2015;7(14):6380-6387. doi:10.1039/c5nr00893j
79. Huang W, Li C, Gao L, et al. Emerging black phosphorus analogue nanomaterials for high-performance device applications. *J Mater Chem C*. 2020;8(4):1172-1197. doi:10.1039/c9tc05558d
80. Xie Z, Wang D, Fan T, et al. Black phosphorus analogue tin sulfide nanosheets: Synthesis and application as near-infrared photothermal agents and drug delivery platforms for cancer therapy. *J Mater Chem B*. 2018;6(29):4747-4755. doi:10.1039/c8tb00729b

81. Liu F, Shimotani H, Shang H, et al. High-Sensitivity Photodetectors Based on Multilayer GaTe Flakes. *ACS Publ.* 2013;8(1):752-760. doi:10.1021/nn4054039
82. Jayakumar A, Surendranath A, PV M. 2D materials for next generation healthcare applications. *Int J Pharm.* 2018;551(1-2):309-321. doi:10.1016/j.ijpharm.2018.09.041
83. Luo M, Fan T, Zhou Y, Zhang H, Mei L. 2D Black Phosphorus–Based Biomedical Applications. *Adv Funct Mater.* 2019;29(13):1-19. doi:10.1002/adfm.201808306
84. Haller C, Hizoh I. The Cytotoxicity of Iodinated Radiocontrast Agents on Renal Cells In Vitro. *Invest Radiol.* 2004;39(3):149-154. doi:10.1097/01.rli.0000113776.87762.49
85. He S, Song J, Qu J, Cheng Z. Crucial breakthrough of second near-infrared biological window fluorophores: Design and synthesis toward multimodal imaging and theranostics. *Chem Soc Rev.* 2018;47(12):4258-4278. doi:10.1039/c8cs00234g
86. H. R C, Schiffman JD, Balakrishna RG. Quantum dots as fluorescent probes: Synthesis, surface chemistry, energy transfer mechanisms, and applications. *Sensors Actuators, B Chem.* 2018;258:1191-1214. doi:10.1016/j.snb.2017.11.189
87. Sun Z, Zhao Y, Li Z, et al. TiL4-Coordinated Black Phosphorus Quantum Dots as an Efficient Contrast Agent for In Vivo Photoacoustic Imaging of Cancer. *Small.* 2017;13(11). doi:10.1002/smll.201602896
88. Qu G, Liu W, Zhao Y, et al. Improved Biocompatibility of Black Phosphorus Nanosheets by Chemical Modification. *Angew Chemie Int Ed.* 2017;56(46):14488-14493. doi:10.1002/anie.201706228
89. Saha RK, Karmakar S, Roy M. Photoacoustic examination of red blood cell suspensions *. 2014;(January 2013).
90. Sun C, Wen L, Zeng J, et al. One-pot solventless preparation of PEGylated black phosphorus nanoparticles for photoacoustic imaging and photothermal therapy of cancer. *Biomaterials.* 2016;91:81-89. doi:10.1016/j.biomaterials.2016.03.022
91. Jares-Erijman EA, Jovin TM. FRET imaging. *Nat Biotechnol.* 2003;21(11):1387-1395. doi:10.1038/nbt896
92. Xu M, Wang L V. Photoacoustic imaging in biomedicine. *Rev Sci Instrum.* 2006;77(4). doi:10.1063/1.2195024
93. Cai Y, Wei Z, Song C, Tang C, Han W, Dong X. Optical nano-agents in the second near-infrared window for biomedical applications. *Chem Soc Rev.* 2019;48(1):22-37. doi:10.1039/c8cs00494c
94. Ambrosio A, Tamagnone M, Chaudhary K, et al. Selective excitation and imaging of ultraslow phonon polaritons in thin hexagonal boron nitride crystals. *Light Sci Appl.* 2018;7(1). doi:10.1038/s41377-018-0039-4
95. Zemp RJ, Song L, Bitton R, Shung KK, Wang L V. Realtime photoacoustic microscopy in vivo with a 30-MHz ultrasound array transducer. *Opt Express.* 2008;16(11):7915. doi:10.1364/oe.16.007915

96. Yin J, Tao C, Cai P, Liu X. Photoacoustic tomography based on the Green's function retrieval with ultrasound interferometry for sample partially behind an acoustically scattering layer. *Appl Phys Lett*. 2015;106(23):234101. doi:10.1063/1.4922386
97. Stein EW, Maslov K, Wang L V. Noninvasive, in vivo imaging of the mouse brain using photoacoustic microscopy. *J Appl Phys*. 2009;105(10):102027. doi:10.1063/1.3116134
98. Deng K, Hou Z, Deng X, Yang P, Li C, Lin J. Enhanced Antitumor Efficacy by 808 nm Laser-Induced Synergistic Photothermal and Photodynamic Therapy Based on a Indocyanine-Green-Attached W₁₈O₄₉ Nanostructure. *Adv Funct Mater*. 2015;25(47):7280-7290. doi:10.1002/adfm.201503046
99. Tang Q, Si W, Huang C, et al. An aza-BODIPY photosensitizer for photoacoustic and photothermal imaging guided dual modal cancer phototherapy. *J Mater Chem B*. 2017;5(8):1566-1573. doi:10.1039/c6tb02979e
100. Jia Q, Li D, Zhang Q, et al. Biomineralization synthesis of HBc-CuS nanoparticles for near-infrared light-guided photothermal therapy. *J Mater Sci*. 2019;54(20):13255-13264. doi:10.1007/s10853-019-03613-6
101. Urbanová V, Pumera M. Biomedical and bioimaging applications of 2D pnictogens and transition metal dichalcogenides. *Nanoscale*. 2019;11(34):15770-15782. doi:10.1039/c9nr04658e
102. Kumar M, Singh VP, Dubey S, Suh Y, Park SH. GaN nanophosphors for white-light applications. *Opt Mater (Amst)*. 2018;75:61-67. doi:10.1016/j.optmat.2017.10.021
103. Kosaka N, Ogawa M, Choyke PL, Kobayashi H. Clinical implications of near-infrared fluorescence imaging in cancer. *Futur Oncol*. 2009;5(9):1501-1511. doi:10.2217/fon.09.109
104. Deng G, Li S, Sun Z, et al. Near-infrared fluorescence imaging in the largely unexplored window of 900-1,000 nm. *Theranostics*. 2018;8(15):4116-4128. doi:10.7150/thno.26539
105. Martinić I, Eliseeva S V., Petoud S. Near-infrared emitting probes for biological imaging: Organic fluorophores, quantum dots, fluorescent proteins, lanthanide(III) complexes and nanomaterials. *J Lumin*. 2017;189(Iii):19-43. doi:10.1016/j.jlumin.2016.09.058
106. Brancato R, Trabucchi G. Fluorescein and indocyanine green angiography in vascular chorioretinal diseases. *Semin Ophthalmol*. 1998;13(4):189-198. doi:10.3109/08820539809056052
107. Flower RW, Hochheimer BF. Indocyanine green dye fluorescence and infrared absorption choroidal angiography performed simultaneously with fluorescein angiography. *Johns Hopkins Med J*. 1976;138(2):33-42. Accessed March 31, 2021. <https://europepmc.org/article/med/1249879>
108. Jung JW, Kim C, Cheong JY, Kim ID. Gallium Nitride Nanoparticles Embedded in a Carbon Nanofiber Anode for Ultralong-Cycle-Life Lithium-Ion Batteries. *ACS Appl Mater Interfaces*. 2019;11(47):44263-44269.

doi:10.1021/acsami.9b15231

109. Zhang Y, Zheng Y, Rui K, et al. 2D Black Phosphorus for Energy Storage and Thermoelectric Applications. *Small*. 2017;13(28):1-20. doi:10.1002/sml.201700661
110. Aggarwal N, Gupta G. Enlightening gallium nitride-based UV photodetectors. *J Mater Chem C*. 2020;8(36):12348-12354. doi:10.1039/d0tc03219k
111. Engel M, Steiner M, Avouris P. Black phosphorus photodetector for multispectral, high-resolution imaging. *Nano Lett*. 2014;14(11):6414-6417. doi:10.1021/nl502928y
112. Schäfer S, Wyrzgol SA, Caterino R, et al. Platinum nanoparticles on gallium nitride surfaces: Effect of semiconductor doping on nanoparticle reactivity. *J Am Chem Soc*. 2012;134(30):12528-12535. doi:10.1021/ja3020132
113. Wang HJ, Cao Y, Wu L Le, et al. ZnS-based dual nano-semiconductors (ZnS/PbS, ZnS/CdS or ZnS/Ag₂S₃): A green synthesis route and photocatalytic comparison for removing organic dyes. *J Environ Chem Eng*. 2018;6(6):6771-6779. doi:10.1016/j.jece.2018.10.034
114. Rao MD, Pennathur G. Green synthesis and characterization of cadmium sulphide nanoparticles from *Chlamydomonas reinhardtii* and their application as photocatalysts. *Mater Res Bull*. 2017;85:64-73. doi:10.1016/j.materresbull.2016.08.049
115. Tian B, Tian B, Smith B, et al. Facile bottom-up synthesis of partially oxidized black phosphorus nanosheets as metal-free photocatalyst for hydrogen evolution. *Proc Natl Acad Sci U S A*. 2018;115(17):4345-4350. doi:10.1073/pnas.1800069115
116. Liu D, Wang J, Bian S, et al. Photoelectrochemical Synthesis of Ammonia with Black Phosphorus. *Adv Funct Mater*. 2020;30(24):2002731. doi:10.1002/adfm.202002731
117. Kim D, Shin K, Kwon SG, Hyeon T. Synthesis and Biomedical Applications of Multifunctional Nanoparticles. *Adv Mater*. 2018;30(49):1-26. doi:10.1002/adma.201802309
118. Yao J, Li P, Li L, Yang M. Biochemistry and biomedicine of quantum dots: from biodetection to bioimaging, drug discovery, diagnostics, and therapy. *Acta Biomater*. 2018;74:36-55. doi:10.1016/j.actbio.2018.05.004
119. Rajasekhar A, Gimi B, Hu W. Applications of Semiconductor Fabrication Methods to Nanomedicine: A Review of Recent Inventions and Techniques. *Recent Patents Nanomed*. 2013;3(1):9-20. doi:10.2174/1877912311303010003
120. Wang Y, Zhao Q, Han N, et al. Mesoporous silica nanoparticles in drug delivery and biomedical applications. *Nanomedicine Nanotechnology, Biol Med*. 2015;11(2):313-327. doi:10.1016/j.nano.2014.09.014
121. Khan MAH, Rao M V. Gallium nitride (GaN) nanostructures and their gas sensing properties: A review. *Sensors (Switzerland)*. 2020;20(14):1-22. doi:10.3390/s20143889

122. Jiang QM, Zhang MR, Luo LQ, Pan GB. Electrosynthesis of bismuth nanodendrites/gallium nitride electrode for non-enzymatic hydrogen peroxide detection. *Talanta*. 2017;171:250-254. doi:10.1016/j.talanta.2017.04.075
123. Lan Y, Li J, Wong-Ng W, Derbeshi RM, Li J, Lisfi A. Free-standing self-assemblies of gallium nitride nanoparticles: A review. *Micromachines*. 2016;7(9). doi:10.3390/mi7090121
124. Zhang A, Li A, Zhao W, Liu J. Recent Advances in Functional Polymer Decorated Two-Dimensional Transition-Metal Dichalcogenides Nanomaterials for Chemo-Photothermal Therapy. *Chem - A Eur J*. 2018;24(17):4215-4227. doi:10.1002/chem.201704197
125. Choi H, Johnson JC, He R, et al. Self-Organized GaN Quantum Wire UV Lasers. Published online 2003:8721-8725.
126. Luo Z-C, Liu M, Guo Z-N, et al. Microfiber-based few-layer black phosphorus saturable absorber for ultra-fast fiber laser. *Opt Express*. 2015;23(15):20030. doi:10.1364/oe.23.020030
127. Al-Kattan A, Ryabchikov Y V., Baati T, et al. Ultrapure laser-synthesized Si nanoparticles with variable oxidation states for biomedical applications. *J Mater Chem B*. 2016;4(48):7852-7858. doi:10.1039/c6tb02623k
128. Weng W. Chow SWK. *Semiconductor-Laser Fundamentals: Physics of the Gain Materials - Weng W. Chow, Stephan W. Koch - Google Libros*. Accessed March 31, 2021. [https://books.google.com.ec/books?hl=es&lr=&id=ltEAFxGT3pgC&oi=fnd&pg=PA1&dq=Unlike+conductors,+electrons+in+a+semiconductor+must+obtain+energy+\(ie,+from+ionizing+radiation\)+to+traverse+the+band+gap+and+reach+the+conduction+band.&ots=zSjI0GOKj7&sig=li-bfHlaAarc5-4D-hJQ9S8Avj4#v=onepage&q&f=false](https://books.google.com.ec/books?hl=es&lr=&id=ltEAFxGT3pgC&oi=fnd&pg=PA1&dq=Unlike+conductors,+electrons+in+a+semiconductor+must+obtain+energy+(ie,+from+ionizing+radiation)+to+traverse+the+band+gap+and+reach+the+conduction+band.&ots=zSjI0GOKj7&sig=li-bfHlaAarc5-4D-hJQ9S8Avj4#v=onepage&q&f=false)
129. Huang XW, Wei JJ, Zhang MY, et al. Water-Based Black Phosphorus Hybrid Nanosheets as a Moldable Platform for Wound Healing Applications. *ACS Appl Mater Interfaces*. 2018;10(41):35495-35502. doi:10.1021/acsami.8b12523
130. Zhou J, Yang Y, Zhang CY. Toward Biocompatible Semiconductor Quantum Dots: From Biosynthesis and Bioconjugation to Biomedical Application. *Chem Rev*. 2015;115(21):11669-11717. doi:10.1021/acs.chemrev.5b00049
131. Rossetti R, Hull R, Gibson JM, Brus LE. Excited electronic states and optical spectra of ZnS and CdS crystallites in the ≈ 15 to 50 Å size range: Evolution from molecular to bulk semiconducting properties. *J Chem Phys*. 1985;82(1):552-559. doi:10.1063/1.448727
132. Li J, Zhu JJ. Quantum dots for fluorescent biosensing and bio-imaging applications. *Analyst*. 2013;138(9):2506-2515. doi:10.1039/c3an36705c
133. Martinić I, Eliseeva S, Luminescence SP-J of, 2017 undefined. Near-infrared emitting probes for biological imaging: organic fluorophores, quantum dots, fluorescent proteins, lanthanide (III) complexes and nanomaterials. *Elsevier*. Accessed April 13, 2021. <https://www.sciencedirect.com/science/article/pii/S0022231316308766>

134. Park Y, Jeong S, Kim S. Medically translatable quantum dots for biosensing and imaging. *J Photochem Photobiol C Photochem Rev.* 2017;30:51-70. doi:10.1016/j.jphotochemrev.2017.01.002
135. Gao G, Jiang YW, Sun W, Wu FG. Fluorescent quantum dots for microbial imaging. *Chinese Chem Lett.* 2018;29(10):1475-1485. doi:10.1016/j.ccllet.2018.07.004
136. Razeghi M, Nguyen BM. Advances in mid-infrared detection and imaging: A key issues review. *Reports Prog Phys.* 2014;77(8):082401. doi:10.1088/0034-4885/77/8/082401
137. Smith AM, Gao X, Nie S. Quantum Dot Nanocrystals for In Vivo Molecular and Cellular Imaging. *Photochem Photobiol.* 2007;80(3):377-385. doi:10.1111/j.1751-1097.2004.tb00102.x
138. Kumar S V., Bafana AP, Pawar P, et al. Optimized production of antibacterial copper oxide nanoparticles in a microwave-assisted synthesis reaction using response surface methodology. *Colloids Surfaces A Physicochem Eng Asp.* 2019;573:170-178. doi:10.1016/j.colsurfa.2019.04.063
139. Liu H, Neal AT, Zhu Z, et al. Phosphorene: An unexplored 2D semiconductor with a high hole mobility. *ACS Nano.* 2014;8(4):4033-4041. doi:10.1021/nn501226z
140. Shimada M, Azuma Y, Okuyama K, Hayashi Y, Tanabe E. Plasma Synthesis of Light Emitting Gallium Nitride Nanoparticles Using a Novel Microwave-Resonant Cavity. *Jpn J Appl Phys.* 2006;45(1A):328-332. doi:10.1143/jjap.45.328
141. *Opportunities and Risks of Nanotechnologies Report in Co-Operation with the OECD International Futures Programme.*
142. Kang SH, Bozhilov KN, Myung NV, Mulchandani A, Chen W. Microbial Synthesis of CdS Nanocrystals in Genetically Engineered *E. coli*. *Angew Chemie Int Ed.* 2008;47(28):5186-5189. doi:10.1002/anie.200705806
143. Zhao H, Chaker M, Wu N, Ma D. Towards controlled synthesis and better understanding of highly luminescent PbS/CdS core/shell quantum dots. *J Mater Chem.* 2011;21(24):8898-8904. doi:10.1039/c1jm11205h
144. Zhu C, Chen Z, Gao S, et al. Recent advances in non-toxic quantum dots and their biomedical applications. *Prog Nat Sci Mater Int.* 2019;29(6):628-640. doi:10.1016/j.pnsc.2019.11.007
145. Chen M, Yin M. Design and development of fluorescent nanostructures for bioimaging. *Prog Polym Sci.* 2014;39(2):365-395. doi:10.1016/j.progpolymsci.2013.11.001
146. Alivisatos AP, Harris AL, Levinos NJ, Steigerwald ML, Brus LE. Electronic states of semiconductor clusters: Homogeneous and inhomogeneous broadening of the optical spectrum. *J Chem Phys.* 1988;89(7):4001-4011. doi:10.1063/1.454833
147. Alivisatos AP. Semiconductor clusters, nanocrystals, and quantum dots. *Science (80-).* 1996;271(5251):933-937. doi:10.1126/science.271.5251.933

148. Chinnathambi S, Shirahata N. Recent advances on fluorescent biomarkers of near-infrared quantum dots for in vitro and in vivo imaging. *Sci Technol Adv Mater*. 2019;20(1):337-355. doi:10.1080/14686996.2019.1590731
149. Xu Q, Wan Y, Hu T, Liu T, ... DT-N, 2015 undefined. Robust self-cleaning and micromanipulation capabilities of gecko spatulae and their bio-mimics. *nature.com*. Accessed April 15, 2021. <https://www.nature.com/articles/ncomms9949>
150. Xu Q, Xu H, Chen J, Lv Y, Dong C, Sreeprasad TS. <http://rsc.li/frontiers-inorganic> Graphene and graphene oxide: advanced membranes for gas separation and water purification. *Inorg Chem Front*. 2015;2:417. doi:10.1039/c4qi00230j
151. Xu Q, Zhao J, Liu Y, et al. Enhancing the luminescence of carbon dots by doping nitrogen element and its application in the detection of Fe(III). *J Mater Sci*. 2015;50(6):2571-2576. doi:10.1007/s10853-015-8822-6
152. Xu Q, Kuang T, Liu Y, Cai L, ... XP-J of M, 2016 undefined. Heteroatom-doped carbon dots: synthesis, characterization, properties, photoluminescence mechanism and biological applications. *pubs.rsc.org*. Accessed April 15, 2021. <https://pubs.rsc.org/am/content/articlehtml/2016/tb/c6tb02131j>
153. Ding H, Yu SB, Wei JS, Xiong HM. Full-color light-emitting carbon dots with a surface-state-controlled luminescence mechanism. *ACS Nano*. 2016;10(1):484-491. doi:10.1021/acsnano.5b05406
154. Pan L, Sun S, Zhang L, Jiang K, Nanoscale HL-, 2016 undefined. Near-infrared emissive carbon dots for two-photon fluorescence bioimaging. *pubs.rsc.org*. Accessed April 15, 2021. <https://pubs.rsc.org/ko/content/articlehtml/2016/nr/c6nr05878g>
155. Lan M, Zhao S, Zhang Z, et al. Electronic Supplementary Material Two-photon-excited near-infrared emissive carbon dots as multifunctional agents for fluorescence imaging and photothermal therapy. *Nano Res*. 2017;10(9):3113-3123. doi:10.1007/s12274-017-1528-0
156. Li D, Wang D, Zhao X, et al. Short-wave infrared emitted/excited fluorescence from carbon dots and preliminary applications in bioimaging †. *Cite this Mater Chem Front*. 2018;2:1343. doi:10.1039/c8qm00151k
157. Li D, Jing P, Sun L, et al. CommuniCation 1705913 (1 of 8) Near-Infrared Excitation/Emission and Multiphoton-Induced Fluorescence of Carbon Dots. *Wiley Online Libr*. 2018;30(13). doi:10.1002/adma.201705913
158. science DC-P in materials, 2017 undefined. Recent advances in germanium nanocrystals: Synthesis, optical properties and applications. *Elsevier*. Accessed April 15, 2021. https://www.sciencedirect.com/science/article/pii/S007964251730097X?casa_tok en=5X-JPMERncIAAAAA:dLoArEKhZc5LrSN2bpQv6xTin87FHZcFDTV5g4j72tQIFCY5KBDhNxWMMJqBtou0Cno1UJreUw
159. Karatutlu A, Song M, Wheeler A, Ersoy O, Advances WL-R, 2015 undefined. Synthesis and structure of free-standing germanium quantum dots and their application in live cell imaging. *pubs.rsc.org*. Accessed April 15, 2021.

- https://pubs.rsc.org/en/content/articlehtml/2015/ra/c5ra01529d?casa_token=1B00NISzAv0AAAAA:Y0yOB20Q-mWO7O45mLZKldzUbbfbj0wjLSDT7rJI5CGMHL15wLRIKl3tyqGEufGousOp-6qGKq6DKw
160. Wang L, Reipa V, Blasic J. Silicon Nanoparticles as a Luminescent Label to DNA. *Bioconjug Chem.* 2004;15(2):409-412. doi:10.1021/bc030047k
 161. Yong K, Law W, Hu R, Ye L, ... LL-CS, 2013 undefined. Nanotoxicity assessment of quantum dots: from cellular to primate studies. *pubs.rsc.org*. Accessed April 15, 2021. https://pubs.rsc.org/en/content/articlehtml/2013/cs/c2cs35392j?casa_token=dDEwA8c1YbEAAAAA:b3N_fHkPPawei6zudWcJMNI2gYMc9Jc2U0lgr5DP1sbeL7hFpzx-0e30sOJ_6klmsp0yBXewht3LA
 162. Chandra S, Ghosh B, Beaune G, Nagarajan U, Nanoscale TY-, 2016 undefined. Functional double-shelled silicon nanocrystals for two-photon fluorescence cell imaging: spectral evolution and tuning. *pubs.rsc.org*. Accessed April 15, 2021. <https://pubs.rsc.org/--/content/articlehtml/2016/nr/c6nr01437b>
 163. Poddubny AN, Dohnalová K. Direct band gap silicon quantum dots achieved via electronegative capping. *Phys Rev B - Condens Matter Mater Phys.* 2014;90(24):245439. doi:10.1103/PhysRevB.90.245439
 164. Ghosh B, Takeguchi M, Nakamura J, reports YN-S, 2016 undefined. Origin of the photoluminescence quantum yields enhanced by alkane-termination of freestanding silicon nanocrystals: temperature-dependence of optical. *nature.com*. Accessed April 15, 2021. <https://www.nature.com/articles/srep36951>
 165. Ghosh B, Yamada H, Chinnathambi S, Özbilgin İNG, Shirahata N. Inverted Device Architecture for Enhanced Performance of Flexible Silicon Quantum Dot Light-Emitting Diode. *J Phys Chem Lett.* 2018;9(18):5400-5407. doi:10.1021/acs.jpcclett.8b02278
 166. Dohnalová K, Poddubny A, ... AP-L science &, 2013 undefined. Surface brightens up Si quantum dots: direct bandgap-like size-tunable emission. *nature.com*. Accessed April 15, 2021. <https://www.nature.com/articles/lsa20133>
 167. Liu X, Zhao S, Gu W, et al. Light-Emitting Diodes Based on Colloidal Silicon Quantum Dots with Octyl and Phenylpropyl Ligands. *ACS Appl Mater Interfaces.* 2018;10(6):5959-5966. doi:10.1021/acsami.7b16980
 168. Ghosh B, Hamaoka T, Nemoto Y, Takeguchi M, Shirahata N. Impact of Anchoring Monolayers on the Enhancement of Radiative Recombination in Light-Emitting Diodes Based on Silicon Nanocrystals. *J Phys Chem C.* 2018;122(11):6422-6430. doi:10.1021/acs.jpcc.7b12812
 169. Chinnathambi S, Pi X, Xu M, Delivery NH-J of D, 2015 undefined. Regulation of bifurcated cytokine induction by surface charge of nanoparticles during interaction between CpG oligodeoxynucleotides and toll-like receptor 9. *Elsevier*. Accessed April 15, 2021. https://www.sciencedirect.com/science/article/pii/S1773224715300071?casa_token=IHS1JC_R5fkAAAAA:1eKI_mR-v19m5T63T2PIX5m5537kHWGYYL1NVhnWxciBw9dOHTIXgouHuohC09OG

QAwQGuV4kg

170. Mazzaro R, Romano F, Ceroni P. Long-lived luminescence of silicon nanocrystals: from principles to applications. *Phys Chem Chem Phys*. 2017;19:26507. doi:10.1039/c7cp05208a
171. Sakiyama M, Sugimoto H, Fujii M. Long-lived luminescence of colloidal silicon quantum dots for time-gated fluorescence imaging in the second near infrared window in biological tissue. *Nanoscale*. 2018;10(29):13902-13907. doi:10.1039/c8nr03571g
172. Su Y, Ji X, He Y, Su YY, Ji XY, He Y. Water-Dispersible Fluorescent Silicon Nanoparticles and their Optical Applications. *Wiley Online Libr*. 2016;28(47):10567-10574. doi:10.1002/adma.201601173
173. Dasog M, Kehrle J, Rieger B, Veinot JGC. Silicon nanocrystals and silicon-polymer hybrids: Synthesis, surface engineering, and applications. *Angew Chemie - Int Ed*. 2016;55(7):2322-2339. doi:10.1002/anie.201506065
174. Chandra S, Masuda Y, Shirahata N, Winnik FM. Transition-Metal-Doped NIR-Emitting Silicon Nanocrystals. *Angew Chemie - Int Ed*. 2017;56(22):6157-6160. doi:10.1002/anie.201700436
175. Hori Y, Kano S, Sugimoto H, Imakita K, Fujii M. Size-Dependence of Acceptor and Donor Levels of Boron and Phosphorus Codoped Colloidal Silicon Nanocrystals. *Nano Lett*. 2016;16(4):2615-2620. doi:10.1021/acs.nanolett.6b00225
176. Ni Z, Pi X, Zhou S, et al. 700 wileyonlinelibrary.com Size-Dependent Structures and Optical Absorption of Boron-Hyperdoped Silicon Nanocrystals. *Wiley Online Libr*. 2016;4(5):700-707. doi:10.1002/adom.201500706
177. Sakiyama M, Sugimoto H, Nanoscale MF-, 2018 undefined. Long-lived luminescence of colloidal silicon quantum dots for time-gated fluorescence imaging in the second near infrared window in biological tissue. *pubs.rsc.org*. Accessed April 15, 2021. https://pubs.rsc.org/en/content/articlehtml/2018/nr/c8nr03571g?casa_token=9YpHaNwDeewAAAAA:DaLczu1CehUXBndTRcuP9OWYIQJuAGgoylupHwWKOMWSkRw7-E_1ONkONxUNrtXs6NmW9RpWcj5T
178. Pringle TA, Hunter KI, Brumberg A, et al. Bright Silicon Nanocrystals from a Liquid Precursor: Quasi-Direct Recombination with High Quantum Yield. *ACS Nano*. 2020;14(4):3858-3867. doi:10.1021/acsnano.9b09614
179. Yu Y, Fan G, Fermi A, et al. Size-Dependent Photoluminescence Efficiency of Silicon Nanocrystal Quantum Dots. *J Phys Chem C*. 2017;121(41):23240-23248. doi:10.1021/acs.jpcc.7b08054
180. Sanghaleh F, Sychugov I, Yang Z, Veinot JGC, Linnros J. Near-Unity Internal Quantum Efficiency of Luminescent Silicon Nanocrystals with Ligand Passivation. *ACS Nano*. 2015;9(7):7097-7104. doi:10.1021/acsnano.5b01717
181. Morozova S, Alikina M, Vinogradov A, Pagliaro M. Silicon Quantum Dots: Synthesis, Encapsulation, and Application in Light-Emitting Diodes. *Front Chem*. 2020;8. doi:10.3389/fchem.2020.00191

182. Montalti M, Cantelli A, Battistelli G. Nanodiamonds and silicon quantum dots: ultrastable and biocompatible luminescent nanoprobe for long-term bioimaging. *Chem Soc Rev.* 2015;44:4853. doi:10.1039/c4cs00486h
183. Tu CC, Chen KP, Yang TA, Chou MY, Lin LY, Li YK. Silicon Quantum Dot Nanoparticles with Antifouling Coatings for Immunostaining on Live Cancer Cells. *ACS Appl Mater Interfaces.* 2016;8(22):13714-13723. doi:10.1021/acsami.6b02318
184. Cheng X, Hinde E, Owen DM, et al. Enhancing Quantum Dots for Bioimaging using Advanced Surface Chemistry and Advanced Optical Microscopy: Application to Silicon Quantum Dots (SiQDs). *Adv Mater.* 2015;27(40):6144-6150. doi:10.1002/adma.201503223
185. Wu JJ, Siva Santosh Kumar Kondeti V, Bruggeman PJ, Kortshagen UR. Luminescent, water-soluble silicon quantum dots via micro-plasma surface treatment. *J Phys D Appl Phys.* 2016;49(8). doi:10.1088/0022-3727/49/8/08LT02
186. Yang Z, C Veinot JG. Size-controlled solid state synthesis of luminescent silicon nanocrystals using Stober silica particles Halide perovskites photovoltaics View project Surface Chemistry of Silicon Nanocrystals View project. *pubs.rsc.org.* 2016;14(22):7576-7578. doi:10.1039/C2CE25950H
187. McVey BFP, König D, Cheng X, et al. Synthesis, optical properties and theoretical modelling of discrete emitting states in doped silicon nanocrystals for bioimaging. *Nanoscale.* 2018;10(33):15600-15607. doi:10.1039/c8nr05071f
188. Chen Y, Sun L, Liao F, Dang Q, Shao M. Fluorescent-stable and water-soluble two-component-modified silicon quantum dots and their application for bioimaging. *J Lumin.* 2019;215(February). doi:10.1016/j.jlumin.2019.116644
189. Fujii M, Fujii R, Takada M, Sugimoto H. Silicon Quantum Dot Supraparticles for Fluorescence Bioimaging. *ACS Appl Nano Mater.* 2020;3(6):6099-6107. doi:10.1021/acsanm.0c01295
190. Belinova T, Vrabцова L, Machova I, et al. Silicon Quantum Dots and Their Impact on Different Human Cells. *Phys status solidi.* 2018;255(10):1700597. doi:10.1002/pssb.201700597
191. Chen Y, Sun L, Liao F, Dang Q, Shao M. Fluorescent-stable and water-soluble two-component-modified silicon quantum dots and their application for bioimaging. *J Lumin.* 2019;215(February):116644. doi:10.1016/j.jlumin.2019.116644
192. Bruns O, Bischof T, Harris D, ... DF-N biomedical, 2017 undefined. Next-generation in vivo optical imaging with short-wave infrared quantum dots. *nature.com.* Accessed April 15, 2021. <https://www.nature.com/articles/s41551-017-0056>
193. Synthesis of super bright indium phosphide colloidal quantum dots through thermal diffusion. *nature.com.* Accessed April 15, 2021. <https://www.nature.com/articles/s42004-019-0138-z>
194. Weng Q, Wang X, Wang X, Bando Y, Golberg D. Functionalized hexagonal boron nitride nanomaterials: Emerging properties and applications. *Chem Soc*

- Rev.* 2016;45(14):3989-4012. doi:10.1039/c5cs00869g
195. Qin G, Du A, Sun Q. A theoretical insight into a feasible strategy for the fabrication of borophane. *Phys Chem Chem Phys.* 2018;20(23):16216-16221. doi:10.1039/c8cp01407h
 196. Ma D, Zhao J, Xie J, et al. Ultrathin boron nanosheets as an emerging two-dimensional photoluminescence material for bioimaging. *Nanoscale Horizons.* 2020;5(4):705-713. doi:10.1039/c9nh00698b
 197. Mannix AJ, Zhang Z, Guisinger NP, Yakobson BI, Hersam MC. Borophene as a prototype for synthetic 2D materials development. *Nat Nanotechnol.* 2018;13(6):444-450. doi:10.1038/s41565-018-0157-4
 198. Liu X, Zhang Z, Wang L, Yakobson BI, Hersam MC. Intermixing and periodic self-assembly of borophene line defects. *Nat Mater.* 2018;17(9):783-788. doi:10.1038/s41563-018-0134-1
 199. Gao N, Wu X, Jiang X, Bai Y, Zhao J. Structure and stability of bilayer borophene: The roles of hexagonal holes and interlayer bonding. *FlatChem.* 2018;7:48-54. doi:10.1016/j.flatc.2017.08.008
 200. Reineck P, Gibson BC. Near-Infrared Fluorescent Nanomaterials for Bioimaging and Sensing. *Adv Opt Mater.* 2017;5(2):1600446. doi:10.1002/adom.201600446
 201. Dobrzhinetskaya LF, Wirth R, Yang J, et al. Qingsongite, natural cubic boron nitride: The first boron mineral from the Earth's mantle. *Am Mineral.* 2014;99(4):764-772. doi:10.2138/am.2014.4714
 202. Jiang XF, Weng Q, Wang X Bin, et al. Recent Progress on Fabrications and Applications of Boron Nitride Nanomaterials: A Review. *J Mater Sci Technol.* 2015;31(6):589-598. doi:10.1016/j.jmst.2014.12.008
 203. Liu B, Yan S, Song Z, et al. One-Step Synthesis of Boron Nitride Quantum Dots: Simple Chemistry Meets Delicate Nanotechnology. *Chem - A Eur J.* 2016;22(52):18899-18907. doi:10.1002/chem.201603935
 204. Chen X, Boulos RA, Dobson JF, Raston CL. Shear induced formation of carbon and boron nitride nano-scrolls. *Nanoscale.* 2013;5(2):498-502. doi:10.1039/c2nr33071g
 205. Hwang DY, Suh DH. Formation of hexagonal boron nitride nanoscrolls induced by inclusion and exclusion of self-assembling molecules in solution process. *Nanoscale.* 2014;6(11):5686-5690. doi:10.1039/c4nr00897a
 206. Hwang DY, Choi KH, Park JE, Suh DH. Evolution of magnetism by rolling up hexagonal boron nitride nanosheets tailored with superparamagnetic nanoparticles. *Phys Chem Chem Phys.* 2017;19(5):4048-4055. doi:10.1039/c6cp08353f
 207. Kumar V, Lahiri D, Lahiri I. Synthesis of Boron Nitride Nanotubes and Boron Nitride Nanoflakes with Potential Application in Bioimaging. *Mater Today Proc.* 2018;5(8):16756-16762. doi:10.1016/j.matpr.2018.06.037
 208. Ge X, Xia Z, Guo S. Recent Advances on Black Phosphorus for Biomedicine and Biosensing. *Adv Funct Mater.* 2019;29(29):1-32. doi:10.1002/adfm.201900318

209. Gui R, Jin H, Wang Z, Li J. Black phosphorus quantum dots: Synthesis, properties, functionalized modification and applications. *Chem Soc Rev.* 2018;47(17):6795-6823. doi:10.1039/c8cs00387d
210. Kalay S, Stetsyshyn Y, Donchak V, et al. pH-Controlled fluorescence switching in water-dispersed polymer brushes grafted to modified boron nitride nanotubes for cellular imaging. *Beilstein J Nanotechnol.* 2019;10:2428-2439. doi:10.3762/bjnano.10.233
211. Tiano AL, Park C, Lee JW, et al. Boron nitride nanotube: synthesis and applications. In: Varadan VK, ed. *Nanosensors, Biosensors, and Info-Tech Sensors and Systems 2014*. Vol 9060. SPIE; 2014:906006. doi:10.1117/12.2045396
212. Cohen ML, Zettl A. The physics of boron nitride nanotubes. *Phys Today.* 2010;63(11):34-38. doi:10.1063/1.3518210
213. Xue Y, Dai P, Zhou M, et al. Multifunctional Superelastic Foam-Like Boron Nitride Nanotubular Cellular-Network Architectures. *ACS Nano.* 2017;11(1):558-568. doi:10.1021/acsnano.6b06601
214. Ling J, Miao X, Sun Y, et al. Vibrational Imaging and Quantification of Two-Dimensional Hexagonal Boron Nitride with Stimulated Raman Scattering. *ACS Nano.* Published online 2019. doi:10.1021/acsnano.9b06337
215. Palombo Blascetta N, Liebel M, Lu X, et al. Nanoscale Imaging and Control of Hexagonal Boron Nitride Single Photon Emitters by a Resonant Nanoantenna. *Nano Lett.* 2020;20(3):1992-1999. doi:10.1021/acs.nanolett.9b05268
216. McLean B, Webber GB, Webber GB, Page AJ. Energy and Charge Transfer at the Boron Nitride Nanotube - Catalyst Growth Interface. *J Phys Chem C.* 2020;124(21):11662-11668. doi:10.1021/acs.jpcc.0c00748
217. Qin X, Yan B, Yu J, et al. Phosphorus-based materials for high-performance rechargeable batteries. *Inorg Chem Front.* 2017;4(9):1424-1444. doi:10.1039/c7qi00184c
218. McLean B, Webber GB, Page AJ. Boron Nitride Nanotube Nucleation during Ni-Catalyzed Boron Oxide Chemical Vapor Deposition. *J Phys Chem C.* Published online 2019. doi:10.1021/acs.jpcc.9b07337
219. Lee CH, Xie M, Kayastha V, Wang J, Yap YK. Patterned growth of boron nitride nanotubes by catalytic chemical vapor deposition. *Chem Mater.* 2010;22(5):1782-1787. doi:10.1021/cm903287u
220. Ge S, Zhang L, Wang P, Fang Y. Intense, stable and excitation wavelength-independent photoluminescence emission in the blue-violet region from phosphorene quantum dots. *Sci Rep.* 2016;6(1):1-6. doi:10.1038/srep27307
221. Wang Y, Si B, Lu S, Liu E, Hu X, Fan J. Near-infrared excitation of CdTe quantum dots based on fluorescence resonance energy transfer and their use as fluorescent sensors. *Sensors Actuators, B Chem.* 2017;246:127-135. doi:10.1016/j.snb.2017.02.069
222. Hu R, Yong KT, Roy I, et al. Functionalized near-infrared quantum dots for in vivo tumor vasculature imaging. *Nanotechnology.* 2010;21(14).

doi:10.1088/0957-4484/21/14/145105

223. Qian H, Dong C, Peng J, Qiu X, Xu Y, Ren J. High-quality and water-soluble near-infrared photoluminescent CdHgTe/CdS quantum dots prepared by adjusting size and composition. *J Phys Chem C*. 2007;111(45):16852-16857. doi:10.1021/jp074961c
224. Yong K, Roy I, Law W, communications RH-C, 2010 undefined. Synthesis of cRGD-peptide conjugated near-infrared CdTe/ZnSe core-shell quantum dots for in vivo cancer targeting and imaging. *pubs.rsc.org*. Accessed April 11, 2021. <https://pubs.rsc.org/ko/content/articlehtml/2010/cc/c0cc00667j>
225. Zhang P, Wan Q. Ultrasmall paramagnetic near infrared quantum dots as dual modal nanoprobes. *pubs.rsc.org*. doi:10.1039/c3ra40995c
226. Zhang P, Hu D, Gong P, et al. A fast synthesis of near-infrared emitting CdTe/CdSe quantum dots with small hydrodynamic diameter for in vivo imaging probes. *pubs.rsc.org*. Published online 2011. doi:10.1039/c1nr10933b
227. Geiregat P, Houtepen AJ, Kishore Sagar L, et al. Continuous-wave infrared optical gain and amplified spontaneous emission at ultralow threshold by colloidal HgTe quantum dots. *nature.com*. Published online 2018. doi:10.1038/NMAT5000
228. He Y, Zhong Y, Su Y, et al. Water-Dispersed Near-Infrared-Emitting Quantum Dots of Ultrasmall Sizes for In Vitro and In Vivo Imaging. *Angew Chemie*. 2011;123(25):5813-5816. doi:10.1002/ange.201004398
229. Chen X, Guo Z, Miao P. One-pot synthesis of GSH-Capped CdTe quantum dots with excellent biocompatibility for direct cell imaging. *Heliyon*. 2018;4(3):e00576. doi:10.1016/j.heliyon.2018.e00576
230. Liu X, Zhou P, Liu H, et al. Design of bright near-infrared-emitting quantum dots capped with different stabilizing ligands for tumor targeting. *pubs.rsc.org*. Accessed April 11, 2021. <https://pubs.rsc.org/en/content/articlehtml/2018/ra/c7ra10824a>
231. Tao J, Zeng Q, Chemical LW-S and AB, 2016 undefined. Near-infrared quantum dots based fluorescent assay of Cu²⁺ and in vitro cellular and in vivo imaging. *Elsevier*. Accessed April 11, 2021. <https://www.sciencedirect.com/science/article/pii/S0925400516307079>
232. Qu M, Qiu Y, Lv R, et al. Exposure to MPA-capped CdTe quantum dots causes reproductive toxicity effects by affecting oogenesis in nematode *Caenorhabditis elegans*. *Ecotoxicol Environ Saf*. 2019;173:54-62. doi:10.1016/j.ecoenv.2019.02.018
233. He K, Liang X, Wei T, et al. DNA damage in BV-2 cells: An important supplement to the neurotoxicity of CdTe quantum dots. *J Appl Toxicol*. 2019;39(3):525-539. doi:10.1002/jat.3745
234. Jie G, Gao X, Ge J, Li C. Multifunctional DNA nanocage with CdTe quantum dots for fluorescence detection of human 8-oxoG DNA glycosylase 1 and doxorubicin delivery to cancer cells. *Microchim Acta*. 2019;186(2):1-9. doi:10.1007/s00604-018-3199-2

235. HELAN P, Mohanraj K, ... GSNMS of, 2015 undefined. Synthesis and characterization of β -Ag₂Se and β -AgCuSe nanoparticles via facile precipitation route. *Elsevier*. Accessed April 15, 2021. <https://www.sciencedirect.com/science/article/pii/S1003632615638365>
236. Tang H, Yang ST, Yang YF, et al. Blood Clearance, Distribution, Transformation, Excretion, and Toxicity of Near-Infrared Quantum Dots Ag₂Se in Mice. *ACS Appl Mater Interfaces*. 2016;8(28):17859-17869. doi:10.1021/acsami.6b05057
237. Wu T, Liang X, He K, et al. The role of NLRP3 inflammasome activation in the neuroinflammatory responses to Ag₂Se quantum dots in microglia. *Nanoscale*. 2019;11(43):20820-20836. doi:10.1039/c9nr06778g
238. Gui R, Sun J, Liu D, Wang Y, Transactions HJ-D, 2014 undefined. Retracted Article: A facile cation exchange-based aqueous synthesis of highly stable and biocompatible Ag₂S quantum dots emitting in the second near-infrared. *pubs.rsc.org*. Accessed April 15, 2021. https://pubs.rsc.org/doi/c4dt00699b?casa_token=5Wnm1NRwNHYAAAAA:GGrh6fj_1KW1BK0fh0_pjNn6UObQw-A0U7cIQpyJSDycTOrygeOI9IBHLb17dFnlefMRC9luQak_MQ
239. Song J, Ma C, Zhang W, et al. Bandgap and Structure Engineering via Cation Exchange: From Binary Ag₂S to Ternary AgInS₂, Quaternary AgZnInS alloy and AgZnInS/ZnS Core/Shell Fluorescent Nanocrystals for Bioimaging. *ACS Publ*. 2016;8(37):24826-24836. doi:10.1021/acsami.6b07768
240. Javidi J, Haeri A, Shirazi F, ... FK-J of C, 2017 undefined. Synthesis, Characterization, In Vivo Imaging, Hemolysis, and Toxicity of Hydrophilic Ag₂S Near-Infrared Quantum Dots. *Springer*. Accessed April 15, 2021. <https://link.springer.com/content/pdf/10.1007/s10876-016-1060-5.pdf>
241. Ge X, Zhang Z, Xie Z, Cui R, Chemistry DP-NJ of, 2017 undefined. Revealing the biodistribution and clearance of Ag₂Se near-infrared quantum dots in mice. *pubs.rsc.org*. Accessed April 15, 2021. <https://pubs.rsc.org/no/content/articlehtml/2017/nj/c7nj02126g>
242. Duman F, Hocaoglu I, Ozturk D, Gozuacik D, Nanoscale AK-, 2015 undefined. Highly luminescent and cytocompatible cationic Ag₂S NIR-emitting quantum dots for optical imaging and gene transfection. *pubs.rsc.org*. Accessed April 15, 2021. https://pubs.rsc.org/en/content/articlehtml/2015/nr/c5nr00189g?casa_token=SWc3Vio_6REAAAAA:lQd0UNpDSOHTqJ86Boo3BYwEAUeH8xVoJX59G9CDWVvIkB5qWgzajBssXuPzNX80ysyXkyVaRZS44w
243. Duman F, Khodadust R, Durmusoglu E, ... MY-R, 2016 undefined. Impact of reaction variables and PEI/l-cysteine ratio on the optical properties and cytocompatibility of cationic Ag₂S quantum dots as NIR bio-imaging probes. *pubs.rsc.org*. Accessed April 15, 2021. https://pubs.rsc.org/en/content/articlehtml/2016/ra/c6ra13804g?casa_token=VLR F9auNnsoAAAAA:Zod6sgRU4eGezop6XHClj9KBmk1hxHtQvHBIwFusi3y9Crxcw51JtKG6wa3XNm09iDJInzQxgJppIQ
244. Shi L, Zhu C, He H, et al. Near-infrared Ag₂Se quantum dots with distinct

- absorption features and high fluorescence quantum yields. *pubs.rsc.org*. Accessed April 15, 2021. <https://pubs.rsc.org/--/content/articlehtml/2016/ra/c6ra04987g>
245. Theodorou IG, Jawad Z, Qin H, et al. Significant metal enhanced fluorescence of Ag₂S quantum dots in the second near-infrared window. *Nanoscale*. Published online 2016. doi:10.1039/C6NR03220F
 246. Chen G, Zhang Y, Li C, Huang D, Wang Q, Wang Q. Recent Advances in Tracking the Transplanted Stem Cells Using Near-Infrared Fluorescent Nanoprobes: Turning from the First to the Second Near-Infrared Window. *Wiley Online Libr*. Published online 2018. doi:10.1002/adhm.201800497
 247. Torimoto T, Kameyama T, Kuwabata S. Photofunctional materials fabricated with chalcopyrite-type semiconductor nanoparticles composed of AgInS₂ and its solid solutions. *J Phys Chem Lett*. 2014;5(2):336-347. doi:10.1021/jz402378x
 248. Mao B, Chuang CH, McCleese C, Zhu J, Burda C. Near-infrared emitting AgInS₂/ZnS nanocrystals. *J Phys Chem C*. 2014;118(25):13883-13889. doi:10.1021/jp500872w
 249. Xi Y, Yang J, Ge Y, et al. One-pot synthesis of water-soluble near-infrared fluorescence RNase A capped CuInS₂ quantum dots for in vivo imaging. *pubs.rsc.org*. Accessed April 15, 2021. <https://pubs.rsc.org/ko/content/articlehtml/2017/ra/c7ra08418h>
 250. Tan L, Liu S, Li X, Chronakis I, B YS-C and S, 2015 undefined. A new strategy for synthesizing AgInS₂ quantum dots emitting brightly in near-infrared window for in vivo imaging. *Elsevier*. Accessed April 15, 2021. https://www.sciencedirect.com/science/article/pii/S0927776514006663?casa_token=riTxvzZTjoEAAAAA:z2__oaStWoCXcpJyjphQzMhlysoX08xgSuz5-xGjwQsQ3pZwFUW3yLi5hK4WzKuNf5A9a7-uhA
 251. Fahmi M, Chemistry JC-P, 2016 undefined. Potential application of oleylamine-encapsulated AgInS₂-ZnS quantum dots for cancer cell labeling. *Elsevier*. Accessed April 15, 2021. <https://www.sciencedirect.com/science/article/pii/S187661961600019X>
 252. Che D, Zhu X, Wang H, Duan Y, ... QZ-J of colloid and, 2016 undefined. Aqueous synthesis of high bright and tunable near-infrared AgInSe₂-ZnSe quantum dots for bioimaging. *Elsevier*. Accessed April 15, 2021. https://www.sciencedirect.com/science/article/pii/S0021979715302848?casa_token=ULqNxF-OD14AAAAA:fAccf4cbH7VklspEV4MOtHzD2UkjHthV7N2maRQYQ9SNIR2vMdgArwbE5AmsF7fgKRT_bG_uCw
 253. Semonin OE, Johnson JC, Luther JM, Midgett AG, Nozik AJ, Beard MC. Absolute photoluminescence quantum yields of IR-26 Dye, PbS, and PbSe quantum dots. *J Phys Chem Lett*. 2010;1(16):2445-2450. doi:10.1021/jz100830r
 254. Lignos I, Protesescu L, Stavrakis S, et al. Facile droplet-based microfluidic synthesis of monodisperse IV-VI semiconductor nanocrystals with coupled in-line NIR fluorescence detection. *Chem Mater*. 2014;26(9):2975-2982. doi:10.1021/cm500774p

255. Benayas A, Ren F, Carrasco E, et al. PbS/CdS/ZnS Quantum Dots: A Multifunctional Platform for In Vivo Near-Infrared Low-Dose Fluorescence Imaging. *Adv Funct Mater.* 2015;25(42):6650-6659. doi:10.1002/adfm.201502632
256. Zhao P, He K, Han Y, et al. Near-Infrared Dual-Emission Quantum Dots-Gold Nanoclusters Nanohybrid via Co-Template Synthesis for Ratiometric Fluorescent Detection and Bioimaging of Ascorbic Acid In Vitro and In Vivo. *Anal Chem.* 2015;87(19):9998-10005. doi:10.1021/acs.analchem.5b02614
257. Imamura Y, Yamada S, Tsuboi S, et al. molecules Near-Infrared Emitting PbS Quantum Dots for in Vivo Fluorescence Imaging of the Thrombotic State in Septic Mouse Brain. *mdpi.com*. Published online 2016. doi:10.3390/molecules21081080
258. Zamberlan F, Turyanska L, Patanè A, et al. Stable DHLA-PEG capped PbS quantum dots: From synthesis to near-infrared biomedical imaging. *J Mater Chem B.* 2018;6(4):550-555. doi:10.1039/c7tb02912h
259. Tatullo M, Genovese F, Aiello E, et al. Phosphorene is the new graphene in biomedical applications. *Materials (Basel).* 2019;12(14). doi:10.3390/ma12142301
260. Ling X, Wang H, Huang S, Xia F, Dresselhaus MS. The renaissance of black phosphorus. *Proc Natl Acad Sci U S A.* 2015;112(15):4523-4530. doi:10.1073/pnas.1416581112
261. Smith JB, Hagaman D, Ji HF. Growth of 2D black phosphorus film from chemical vapor deposition. *Nanotechnology.* 2016;27(21). doi:10.1088/0957-4484/27/21/215602
262. Pica M, D'Amato R. Chemistry of Phosphorene: Synthesis, Functionalization and Biomedical Applications in an Update Review. *Inorganics.* 2020;8(4):29. doi:10.3390/inorganics8040029
263. Kou L, Chen C, Smith SC. Phosphorene: Fabrication, properties, and applications. *J Phys Chem Lett.* 2015;6(14):2794-2805. doi:10.1021/acs.jpcclett.5b01094
264. Smith JB, Hagaman D, Ji H. Growth of 2D black phosphorus film from chemical vapor deposition. *Nanotechnology.* 2016;27(21):1-8. doi:10.1088/0957-4484/27/21/215602
265. Shin YC, Song SJ, Lee Y Bin, et al. Application of black phosphorus nanodots to live cell imaging. *Biomater Res.* 2018;22(1):31. doi:10.1186/s40824-018-0142-x
266. Fu H, Li Z, Xie H, et al. Different-sized black phosphorus nanosheets with good cytocompatibility and high photothermal performance. *RSC Adv.* 2017;7(24):14618-14624. doi:10.1039/c7ra00160f
267. Zhang Y, Zheng Y, Rui K, et al. 2D Black Phosphorus for Energy Storage and Thermoelectric Applications. *Small.* 2017;13(28):1700661. doi:10.1002/smll.201700661
268. Ma J, Lu S, Guo Z, et al. Few-layer black phosphorus based saturable absorber mirror for pulsed solid-state lasers. *Opt Express.* 2015;23(17):22643.

doi:10.1364/oe.23.022643

269. Kang J, Wood JD, Wells SA, et al. Solvent exfoliation of electronic-grade, two-dimensional black phosphorus. *ACS Nano*. 2015;9(4):3596-3604. doi:10.1021/acsnano.5b01143
270. Cheng GS, Zhang LD, Zhu Y, et al. Large-scale synthesis of single crystalline gallium nitride nanowires. *Appl Phys Lett*. 1999;75(16):2455-2457. doi:10.1063/1.125046
271. Zhang J, Shin H, Lu W. Highly ambient-stable few-layer black phosphorene by pulsed laser exfoliation and HEMM. *Chem Commun*. 2019;55(18):2601-2604. doi:10.1039/c8cc09174a
272. Zhang Y, Rui X, Tang Y, et al. Wet-chemical processing of phosphorus composite nanosheets for high-rate and high-capacity lithium-ion batteries. *Adv Energy Mater*. 2016;6(10). doi:10.1002/aenm.201502409
273. Lee HU, Park SY, Lee SC, et al. Black Phosphorus (BP) Nanodots for Potential Biomedical Applications. *Small*. 2016;12(2):214-219. doi:10.1002/sml.201502756
274. Lee HU, Park SY, Lee SC, et al. Black Phosphorus (BP) Nanodots for Potential Biomedical Applications. 2016;(2):214-219. doi:10.1002/sml.201502756
275. Tao W, Zhu X, Yu X, et al. Black Phosphorus Nanosheets as a Robust Delivery Platform for Cancer Theranostics. *Adv Mater*. 2017;29(1):1-9. doi:10.1002/adma.201603276
276. Buscema M, Groenendijk DJ, Steele GA, Van Der Zant HSJ, Castellanos-Gomez A. Photovoltaic effect in few-layer black phosphorus PN junctions defined by local electrostatic gating. *Nat Commun*. 2014;5:4651. doi:10.1038/ncomms5651
277. Hu L, Amini MN, Wu Y, et al. Charge Transfer Doping Modulated Raman Scattering and Enhanced Stability of Black Phosphorus Quantum Dots on a ZnO Nanorod. *Adv Opt Mater*. 2018;6(15):1-10. doi:10.1002/adom.201800440
278. Tao W, Zhu X, Yu X, et al. Black Phosphorus Nanosheets as a Robust Delivery Platform for Cancer Theranostics. *Adv Mater*. 2017;29(1):1603276. doi:10.1002/adma.201603276
279. Qiu M, Ren WX, Jeong T, et al. Omnipotent phosphorene: a next-generation, two-dimensional nanoplatform for multidisciplinary biomedical applications. *Chem Soc Rev*. 2018;47(15):5588-5601. doi:10.1039/c8cs00342d
280. Chen W, Ouyang J, Liu H, et al. Black Phosphorus Nanosheet-Based Drug Delivery System for Synergistic Photodynamic/Photothermal/Chemotherapy of Cancer. *Adv Mater*. 2017;29(5). doi:10.1002/adma.201603864
281. Smith JB, Hagaman D, Ji H, et al. Defining the role of humidity in the ambient degradation of few-layer black phosphorus. *2D Mater*. 2016;4(1):1-8. doi:10.1088/2053-1583/4/1/015025
282. Ryder CR, Wood JD, Wells SA, et al. Covalent functionalization and passivation of exfoliated black phosphorus via aryl diazonium chemistry. *Nat Chem*. 2016;8(6):597-602. doi:10.1038/nchem.2505

283. Yang X, Wang D, Shi Y, et al. Black Phosphorus Nanosheets Immobilizing Ce6 for Imaging-Guided Photothermal/Photodynamic Cancer Therapy. *ACS Appl Mater Interfaces*. 2018;10(15):12431-12440. doi:10.1021/acsami.8b00276
284. Shao J, Xie H, Huang H, et al. Biodegradable black phosphorus-based nanospheres for in vivo photothermal cancer therapy. *Nat Commun*. 2016;7(1):1-13. doi:10.1038/ncomms12967
285. Walia S, Sabri Y, Ahmed T, et al. Defining the role of humidity in the ambient degradation of few-layer black phosphorus. *2D Mater*. 2017;4(1). doi:10.1088/2053-1583/4/1/015025
286. Yang G, Liu Z, Li Y, et al. Facile synthesis of black phosphorus-Au nanocomposites for enhanced photothermal cancer therapy and surface-enhanced Raman scattering analysis. *Biomater Sci*. 2017;5(10):2048-2055. doi:10.1039/c7bm00414a
287. Jagannadham K, Howe J, Allard LF. Laser physical vapor deposition of nanocrystalline dots using nanopore filters. *Appl Phys A Mater Sci Process*. 2010;98(2):285-292. doi:10.1007/s00339-009-5432-7
288. Hui L, Han L, Li L, Yang J. Gain High-Quality Colloidal Quantum Dots Directly from Natural Minerals. *ACS Publ*. 2015;31(8):2251-2255. doi:10.1021/la5044415
289. Yang J, Ling T, Wu W, et al. A top-down strategy towards monodisperse colloidal lead sulphide quantum dots. *nature.com*. Accessed April 15, 2021. <https://www.nature.com/articles/ncomms2637>
290. Zeng H, Yang S, Cai W. Reshaping formation and luminescence evolution of ZnO quantum dots by laser-induced fragmentation in liquid. *J Phys Chem C*. 2011;115(12):5038-5043. doi:10.1021/jp109010c
291. Cui R, Liu H-H, Xie H-Y, et al. Living Yeast Cells as a Controllable Biosynthesizer for Fluorescent Quantum Dots. *Adv Funct Mater*. 2009;19(15):2359-2364. doi:10.1002/adfm.200801492
292. Korbekandi H, Irvani S, Abbasi S. Production of nanoparticles using organisms. *Crit Rev Biotechnol*. 2009;29(4):279-306. doi:10.3109/07388550903062462
293. Wagner AM, Knipe JM, Orive G, Peppas NA. Quantum dots in biomedical applications. *Acta Biomater*. 2019;94(May):44-63. doi:10.1016/j.actbio.2019.05.022
294. Deng D, Zhang W, Chen X, et al. Facile synthesis of high-quality, water-soluble, near-infrared-emitting PbS quantum dots. *Eur J Inorg Chem*. 2009;(23):3440-3446. doi:10.1002/ejic.200900227
295. Durmusoglu EG, Turker Y, Yagci Acar H. Green Synthesis of Strongly Luminescent, Ultrasmall PbS and PbSe Quantum Dots. *ACS Publ*. 2017;121(22):12407-12415. doi:10.1021/acs.jpcc.7b01083
296. Caires AJ, Mansur AAP, Carvalho IC, Carvalho SM, Mansur HS. Green synthesis of ZnS quantum dot/biopolymer photoluminescent nanoprobe for bioimaging brain cancer cells. *Mater Chem Phys*. 2020;244:122716.

doi:10.1016/j.matchemphys.2020.122716

297. Qi K, Wang Y, Wang R, Wu D, C GL-J of MC, 2016 undefined. Facile synthesis of homogeneous CuInS₂ quantum dots with tunable near-infrared emission. *pubs.rsc.org*. Accessed April 15, 2021. <https://pubs.rsc.org/en/content/articlehtml/2016/tc/c5tc04232a>
298. Li L, Zhang R, Lu C, et al. In situ synthesis of NIR-light emitting carbon dots derived from spinach for bio-imaging applications. *pubs.rsc.org*. Accessed April 15, 2021. <https://pubs.rsc.org/en/content/articlehtml/2017/tb/c7tb00634a>
299. Oliveira E, Santos HM, Jorge S, et al. Sustainable synthesis of luminescent CdTe quantum dots coated with modified silica mesoporous nanoparticles: Towards new protein scavengers and smart drug delivery carriers. *Dye Pigment*. 2019;161:360-369. doi:10.1016/j.dyepig.2018.09.047
300. García DA, Mendoza L, Vizuete K, et al. Sugar-Mediated Green Synthesis of Silver Selenide Semiconductor Nanocrystals under Ultrasound Irradiation. *Molecules*. 2020;25(21):5193. doi:10.3390/molecules25215193
301. Vijaya Bharathi M, Maiti S, Sarkar B, Ghosh K, Paira P. Water-mediated green synthesis of Pbs quantum dot and its glutathione and biotin conjugates for non-invasive live cell imaging. *R Soc Open Sci*. 2018;5(3). doi:10.1098/rsos.171614
302. Kharissova O V., Dias HVR, Kharisov BI, Pérez BO, Pérez VMJ. The greener synthesis of nanoparticles. *Trends Biotechnol*. 2013;31(4):240-248. doi:10.1016/j.tibtech.2013.01.003